

# Mechanical properties of 4 rocks at different temperatures and fracture assessment using the strain energy density criterion

J. Justo\*, J. Castro

Group of Geotechnical Engineering, Universidad de Cantabria, E.T.S de Ingenieros de Caminos, Canales y Puertos, Av/ Los Castros 44, 39005, Santander, Spain

## ARTICLE INFO

### Article history:

Received 11 June 2020

Received in revised form 15 July 2020

Accepted 28 July 2020

Available online 30 July 2020

### Editors-in-Chief:

Professor Lyesse Laloui and Professor Tomasz Hueckel

### Keywords:

Strain Energy Density

Temperature

Notch

Rock

Marble

Sandstone

Limestone

## ABSTRACT

This work aims to analyse the fracture behaviour of rocks with U-shaped notches subjected to mode I loading and to different temperature conditions. To this end, an energy-based approach is used called the Strain Energy Density (SED) criterion. This study attempts to extend a previous work of the authors where the SED criterion was successfully applied to U-notched components subjected to mode I loading conditions at room temperature. In this case, the effect of temperature is considered as a new variable.

The research analyses four different types of isotropic rocks with different lithologies, namely a Floresta sandstone, a Moleano limestone, a Macael marble and a Carrara marble. An exhaustive laboratory campaign was performed to define the main mechanical properties of the selected rocks at different temperatures. In total, 144 tensile splitting (Brazilian) tests, 120 uniaxial compression tests, 410 thermal expansion measurements and more than 790 four-point bending tests have been executed under different thermal conditions. On the other hand, the range of temperatures analysed varies from room temperature up to 250 °C, which is a common band in geothermal applications.

Temperature has proven to be a significant parameter when analysing the fracture behaviour of the four selected rocks. Its influence on the main mechanical properties of the rocks (tensile strength, fracture toughness, compressive strength, Young's modulus, Poisson's ratio) has been studied and similar trends have been observed for the marbles, but different or even opposite ones for the sandstone and limestone. Overall, the application of the SED criterion has led to relatively accurate fracture predictions under different temperature conditions. This methodology assumes a linear-elastic behaviour of the rocks at the studied range of temperatures. For this reason, the failure load predictions become less accurate when non-linearities are not negligible, as in the case of the Carrara marble.

© 2020 Elsevier Ltd. All rights reserved.

## 1. Introduction

In several underground engineering fields (e.g., coal mining,<sup>1</sup> geothermal energy,<sup>2</sup> nuclear waste disposal,<sup>3</sup> rock drilling<sup>4</sup>), a deep understanding of the influence of temperature on the brittle response of rocks is a major issue of interest. The mechanical characteristics of rocks can vary significantly with a moderate increase of temperatures up to approximately 250 °C, which is an expected range for conventional high-level radioactive waste disposal<sup>5</sup> and for conventional or hot fracture rock geothermal energy systems.<sup>6</sup> For example, projects dealing with the Enhanced Geothermal System (EGS) technology have been broadly developed and spread since the 1970s.<sup>7</sup> In EGSs, hydraulic fracturing is used to improve well productivity and injectivity in conventional geothermal resources where massive rock blocks are found at temperatures around 250 °C.

The thermal variation of the mechanical properties of rocks has been extensively studied and documented by different authors (e.g., Refs. 6, 8–11). In many cases, these properties are studied after subjecting the rock samples to a thermal treatment or cycle (e.g., Refs. 8, 12), while in other cases (somewhat less usual) the tests are performed under temperature control (e.g., Refs. 11, 13). Besides, the observed mechanisms vary depending on the range of studied temperatures. For moderate temperature increments, a strengthening effect can be observed in some cases.<sup>14</sup> This could be related to the partial closure of pre-existing cracks with thermal expansion<sup>10</sup> or to the dissipation of the stress concentration at crack tips by increased plasticity.<sup>14</sup> This phenomenon is obviously limited and beyond a certain critical temperature, the rocks become weaker as a consequence of thermal cracking.<sup>15</sup> However, in the case of relatively higher temperatures (of the order of several hundred degrees Celsius), an evident resistance loss occurs due to a partial melting<sup>16</sup> and brittle creep<sup>17</sup> of the rocks, even undergoing chemical and microstructural changes.<sup>6</sup>

\* Corresponding author.

E-mail address: [justoj@unican.es](mailto:justoj@unican.es) (J. Justo).

The tensile strength and the fracture toughness are particularly important parameters when analysing the fracture processes of rocks and are significantly affected by temperature. Sirdesai et al.<sup>8</sup> and Dongming and Yushun<sup>12</sup> studied the influence of temperature on a sandstone and a limestone, respectively, and they concluded that changes in the pre-existing pores and microcracks (caused by the internal differential expansion of mineral particles) result in a change in the tensile strength. Similarly, Al-Shayea<sup>18</sup> studied the fracture toughness of a limestone rock formation under different thermal conditions and showed an increase in the fracture toughness up to approximately 120 °C, mainly due to the closure of microcracks or pores caused by the thermal expansion of grains. Meredith and Atkinson<sup>19</sup> related the reduction in the fracture toughness observed in a granite and gabbro to the development of microcracks induced by differential thermal expansions between adjacent mineral particles.

Likewise, Feng et al.<sup>10</sup> reported the case of a sandstone that presented a clear strengthening up to 100°C. Then, a reversal of this trend was observed up to 600 °C, which was the maximum tested temperature. Zhang et al.<sup>15</sup> also performed several uniaxial compression tests of a marble at temperatures between 25 °C and 800 °C. In this case, they found that both the compressive strength and the Young's modulus displayed a general decrease from the onset of the heating process. On the other hand, no clear trends of the thermal effect are usually found on the Poisson's ratio. For example, important differences on the Poisson's ratio of granite can be found in the literature, showing in some cases no thermal effect,<sup>9</sup> or an increasing<sup>20</sup> or decreasing<sup>21</sup> trend, probably because of differences in instruments, testing methods, calculating methods or the diversity of samples.

Together with temperature, the presence of defects like discontinuities, joints, holes, pores, cracks, microcracks or notches play a key role during the fracture initiation processes. These defects, no matter whether they have a natural or man-made origin, act as stress risers, generating stress concentrations around them. Traditional fracture mechanics usually addresses notch problems proceeding on the assumption that they behave as sharp cracks. However, notch-type defects (with a finite radius) develop a higher load-bearing capacity than crack-type defects (with a null radius). Thus, both types of defects should be distinguished for the fracture assessment of rock masses, since assuming that notches behave as cracks may be overly conservative in many cases.<sup>22</sup> Many underground engineering problems (e.g., tunnels, mining, wells) can be generally studied as V-shaped, U-shaped or as intermediate situations like rounded V-notches. For this reason, the influence of the notch geometry on the fracture behaviour of different components has been widely studied (e.g., Refs. 23–25).

Dealing with the brittle fracture of cracked and notched domains, different failure criteria have been proposed in the past by different authors, which may be general or local. Among the local criteria, the most widely used at the moment are probably the Cohesive Zone Model (CZM) (e.g., Refs. 23, 24), Finite Fracture Mechanics (FFM) (e.g., Refs. 26, 27), the Theory of Critical Distances (TCD) (e.g., Refs. 28, 29) and the Strain Energy Density (SED) criterion (e.g., Refs. 30–32). The latter was developed by Lazzarin and co-workers<sup>30,33</sup> based on Neuber's concept of elementary structural volumes.<sup>34</sup> The method states that for a small but finite volume of material close to the notch, whichever its characteristics (blunt notch, sharp notch, corner or crack), the energy always has a finite value. Under this premise, the SED criterion has been successfully applied to brittle or quasi-brittle materials under static and fatigue loading (e.g., Ref. 33), with components weakened by V-notches and U-notches (e.g., Refs. 35, 36) and loaded in pure mode I and mixed mode (e.g., Ref. 36). A recent review was provided by Berto and Lazzarin.<sup>25</sup> For example,

Ayatollahi et al.<sup>37</sup> recently presented some experimental, theoretical and numerical results on the brittle fracture of polycrystalline graphite. The analysis was carried out on V-notched samples under mixed mode loading conditions and based on the Strain Energy Density. Torabi et al.<sup>38</sup> also used the SED criterion for the brittle fracture analysis of key-hole notched PMMA samples under pure mode II loading conditions, obtaining successful failure load predictions. In conclusion, this approach has been successfully applied in the last decades to assess the fracture strength of different materials subjected to wide combinations of static loading conditions. However, scarce work can be found on the application of the SED criterion on rock-type materials (e.g., Refs. 39–41), and to the best of the authors' knowledge, none on the application of the SED criterion on rocks subjected to different temperatures. Berto et al.<sup>39</sup> applied the SED approach to a set of experimental data reported in the literature for the assessment of mixed mode I+II fracture resistance of a Guiting limestone. Likewise, Razavi et al.<sup>41</sup> studied the mixed mode brittle fracture behaviour of granite rock using Asymmetric Four Point Bend specimens, ranging from pure mode I to pure mode II. Finally, Aliha et al.<sup>40</sup> successfully predicted the failure load of a white marble subjected to mixed mode I+II loading conditions by means of the average SED criterion, using inclined edge crack triangular shape rock specimens. All these works only address room temperature fracture conditions.

The authors have previously analysed four different rocks at room temperature using the TCD<sup>22</sup> and SED criterion.<sup>42</sup> Later, this analysis was extended to temperatures up to 250 °C using the TCD.<sup>13</sup> Here, using those same rocks, the analysis is once again extended to apply the SED criterion up to temperatures of 250 °C. The focus is on the fracture assessment of four rocks previously studied by the authors<sup>13</sup> with U-shaped notches under different temperature conditions and subjected to mode I loading. Therefore, the major novelty lies in the evaluation of the applicability of the SED criterion under different temperature conditions. The obtained results, in turn, are compared with those from the TCD analysis.<sup>13</sup> All the required parameters are obtained from an exhaustive experimental program comprising several tensile splitting tests, uniaxial compression tests and four-point bending tests with different notch radii varying from 0.15 mm up to 15 mm, all of them at different temperatures from approximately 23 °C to 250 °C, which is a common range in geothermal applications for example. To this end, the thermal variations of the main mechanical properties of the analysed rocks, which certainly affect the fracture initiation processes of the rocks, are studied in depth.

With all this, Section 2 provides a brief review of the main aspects of the SED criterion. Section 3 describes the analysed rocks and the laboratory tests performed to characterise the material properties. Then, Section 4 includes the obtained results and the discussion concerning the influence of temperature on the main mechanical properties of the rocks: tensile strength, fracture toughness, compressive strength, Young's modulus, Poisson's ratio, thermal dilatation and bending tests. The fracture predictions of the notched rock samples are provided in Section 5. Finally, Section 6 gathers the conclusions of the research.

## 2. Analytical frame: SED criterion

The Strain Energy Density criterion consists of an energy-based failure criterion and states that the average strain energy density ( $\bar{W}$ ) over a well-defined control volume is limited by a critical value ( $W_c$ ).<sup>25</sup> The critical strain energy density  $W_c$  is an intrinsic parameter of the material which, in the case of

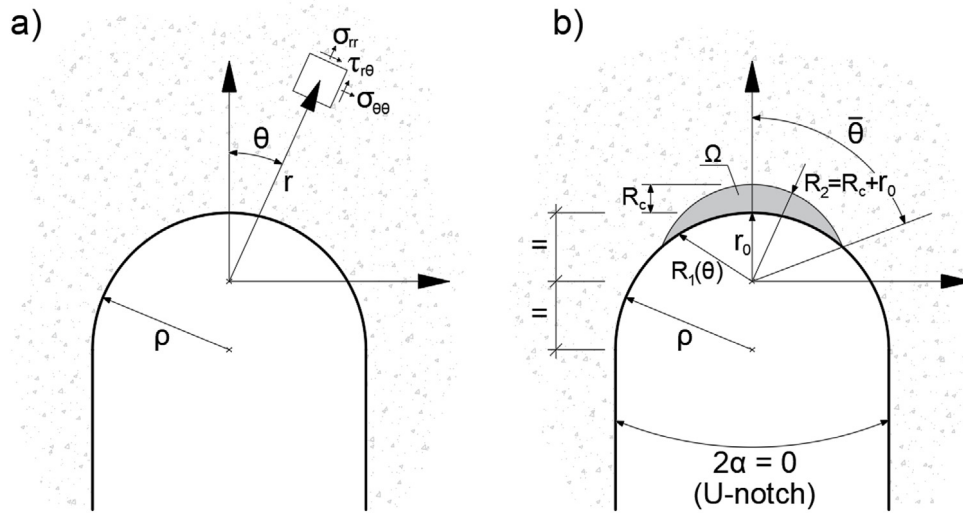


Fig. 1. U-notch under mode I loading conditions: (a) coordinate system; (b) notch geometry and control area  $\Omega$ .

Table 1  
Values of the function H for U-notched specimens.<sup>25</sup>

$R_c/\rho$	$\nu = 0.10$	$\nu = 0.15$	$\nu = 0.20$	$\nu = 0.25$	$\nu = 0.30$	$\nu = 0.35$	$\nu = 0.40$
0.0005	0.6294	0.6215	0.6104	0.5960	0.5785	-	-
0.001	0.6286	0.6207	0.6095	0.5952	0.5777	-	-
0.005	0.6225	0.6145	0.6033	0.5889	0.5714	-	-
0.01	0.6149	0.6068	0.5956	0.5813	0.5638	0.5432	0.5194
0.05	0.5599	0.5515	0.5401	0.5258	0.5086	0.4884	0.4652
0.1	0.5028	0.4942	0.4828	0.4687	0.4518	0.4322	0.4099
0.3	0.3528	0.3445	0.3341	0.3216	0.3069	0.2902	0.2713
0.5	0.2672	0.2599	0.2508	0.2401	0.2276	0.2135	0.1976
1	0.1590	0.1537	0.1473	0.1399	0.1314	0.1217	0.1110

quasi-brittle materials like rocks, is equal to the area under the corresponding linear-elastic stress-strain curve:

$$W_c = \frac{\sigma_u^2}{2E} \quad (1)$$

$\sigma_u$  and  $E$  being the ultimate tensile strength and the Young's modulus of the analysed material, respectively.

On the other hand, the strain energy ( $W$ ) for an isotropic and linear elastic material under plane strain conditions can be calculated at a certain point with the following expression:

$$W(r, \theta, z) = \frac{1}{2E} \{ \sigma_{\theta\theta}^2 + \sigma_{rr}^2 + \sigma_{zz}^2 + 2\tau_{r\theta}^2 - 2\nu(\sigma_{\theta\theta}\sigma_{rr} + \sigma_{\theta\theta}\sigma_{zz} + \sigma_{rr}\sigma_{zz} - \tau_{r\theta}^2) \} \quad (2)$$

where the stress components correspond to the polar coordinates represented in Fig. 1a,  $z$  being the plane strain axis,  $E$  is the Young's modulus and  $\nu$  the Poisson's ratio of the material.

Under plane strain conditions, as those considered in this work, the control volume over which the strain energy is averaged turns into a control area ( $\Omega$ ) that depends on the ultimate tensile strength ( $\sigma_u$ ), the fracture toughness ( $K_{IC}$ ) and the Poisson's ratio ( $\nu$ ) in the case of static loads.<sup>30</sup> Thus,  $\Omega$  is material dependent. Fig. 1b shows a schematic representation of the control area at the notch tip for the particular case of U-shaped notches under mode I loading conditions.

The average strain energy density ( $\bar{W}$ ) over the control area depicted in Fig. 1b can be expressed as follows:

$$\bar{W} = \frac{\int_{\Omega} W d\Omega}{\Omega} = \frac{1}{\Omega} \int_{-\bar{\theta}}^{+\bar{\theta}} d\theta \int_{R_1(\theta)}^{R_2} W(r, \theta) r dr \quad (3)$$

According to the SED criterion,<sup>33,43</sup>  $\Omega$  is defined by a circular sector. In the case of U-shaped notches with a null opening angle

( $2\alpha = 0$ ), this circle is centred at the middle point between the notch tip and the centre of the circle drawing the notch, and is described by a critical length  $R_c$  as shown in Fig. 1b. Yosibah et al.<sup>44</sup> provided the following expression for the calculation of  $R_c$  under plane strain conditions:

$$R_c = \frac{(1 + \nu)(5 - 8\nu)}{4\pi} \left( \frac{K_{IC}}{\sigma_u} \right)^2 \quad (4)$$

Lazzarin and Bertó<sup>30</sup> show in detail the mathematical development of Eq. (3), from which the following expression is derived for the calculation of the average strain energy density:

$$\bar{W} = 0.785 \cdot H \left( \nu, \frac{R_c}{\rho} \right) \cdot \frac{\sigma_{max}^2}{E} \quad (5)$$

where  $\sigma_{max}$  is the maximum stress at the notch tip for a certain load and  $E$  is the Young's modulus of the analysed material. On the other hand, the function  $H$  depends on the Poisson's ratio ( $\nu$ ) and on the ratio  $R_c/\rho$ ,  $\rho$  being the notch radius. This expression is valid for the particular case of U-shaped notches under mode I loading conditions and simplifies to a great extent the fracture assessment of the notched components. Nevertheless, the expressions corresponding to general cases of notches with different opening angles ( $2\alpha$ ) and shapes can also be found in the literature.<sup>25,30,43</sup>

The values for the  $H$  function may be numerically obtained and can be tabulated for a range of  $\nu$  values and  $R_c/\rho$  ratios. For example, the  $H$  values collected in Table 1 correspond to U-shaped notches and were obtained in origin from numerical models with  $\rho = 1$  mm.<sup>25</sup> However, the range of tabulated values available in the literature usually reaches no more than  $R_c/\rho = 1$ , which falls short for rock-type materials as demonstrated by the

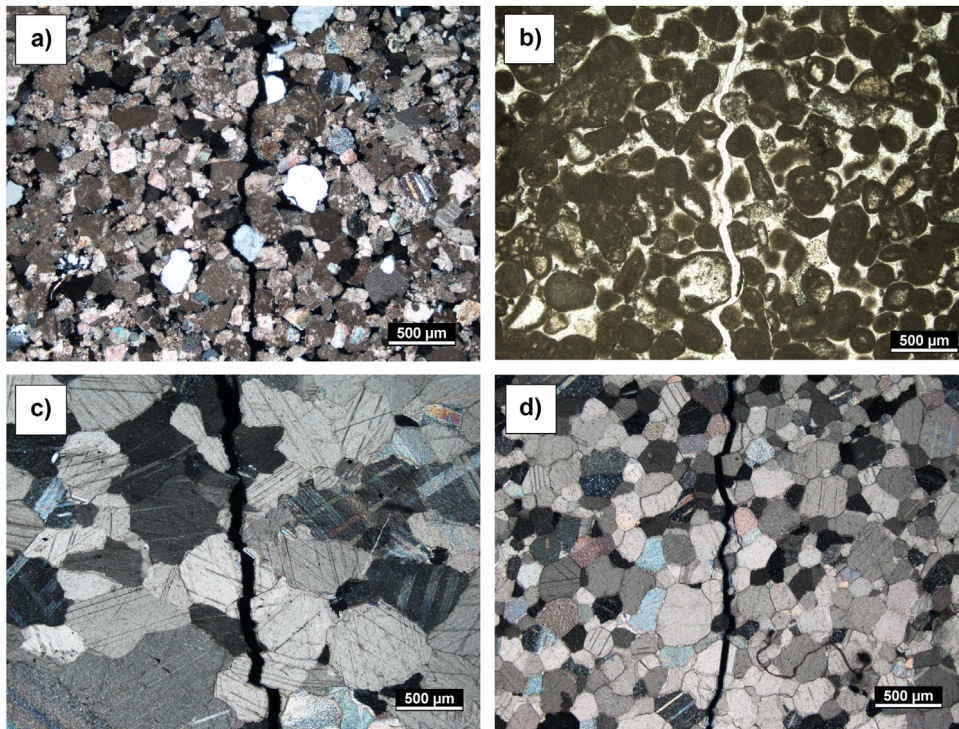


**Fig. 2.** Images of the microstructure of the selected rocks (4x, crossed Nicol): (a) Floresta Sandstone (F), (b) Moleano limestone (C), (c) Macael marble (M), (d) Carrara marble (I).



**Fig. 3.** Experimental set-up of (a) the tensile splitting tests, (b) uniaxial compression tests and (c) four-point bending tests.

authors in a previous work.<sup>42</sup> This range is usually sufficient for materials like steels or polymers (e.g., Refs. 25, 30, 33, 45), where  $R_c$  is relatively small, but in the case of rocks  $R_c$  is of the order of a few millimetres,<sup>42</sup> and therefore, for the range of analysed notch radii,  $R_c/\rho$  reaches higher values up to approximately 45.

Finally, the fracture assessment of the notched rock specimens can be directly made by imposing the average strain energy density in Eq. (5) to be equal to the critical value defined by Eq. (1), which satisfies the failure criterion established by the SED approach ( $\bar{W} = W_c$ ).

### 3. Experimental program

#### 3.1. Analysed rocks

This work focuses on the results of four rocks with different lithologies: a Floresta sandstone (F), a Moleano limestone (C), a Macael marble (M) and a Carrara marble (I). The four selected rocks are predominantly isotropic and relatively homogeneous from a microstructural point of view, which simplifies to a great extent the performed analyses and makes it easier to obtain clear conclusions. The application of the SED criterion has not been fully developed in the field of rocks yet, probably due to the relatively large control areas ( $\Omega$ ) obtained in this type of materials.<sup>42</sup> For this reason, the proposed rock selection aims to cover a broad

range of lithologies and therefore prove the suitability of this methodology in rock fracture assessments, as well as defining its limitations. Fig. 2 displays some images with the microstructure of the four selected rocks, obtained from thin-section analyses with an optical microscope.

Table 2 gathers some technical properties of the rocks at room temperature. A more detailed description of the microstructural composition of these rocks is provided by the authors in a previous work.<sup>22</sup> From the petrographic analyses of the thin-sections, no apparent changes are observed either in the microstructure or composition of the studied rocks after a thermal cycle of 250 °C but for thermal microcracks, which have not been analysed in detail.

#### 3.2. Testing campaign

Apart from the geometrical definition of the specimens, the correct application of the SED criterion requires the characterization of some basic mechanical and deformational parameters of the studied materials, namely the tensile strength ( $\sigma_u$ ), the Young's modulus ( $E$ ), the Poisson's ratio ( $\nu$ ) and the fracture toughness ( $K_{IC}$ ). To do so, several laboratory tests have been performed, both at room temperature and at higher temperatures up to 250 °C. Fig. 3 shows the experimental set-up of the performed tensile splitting (Brazilian) tests (Fig. 3a), uniaxial compression

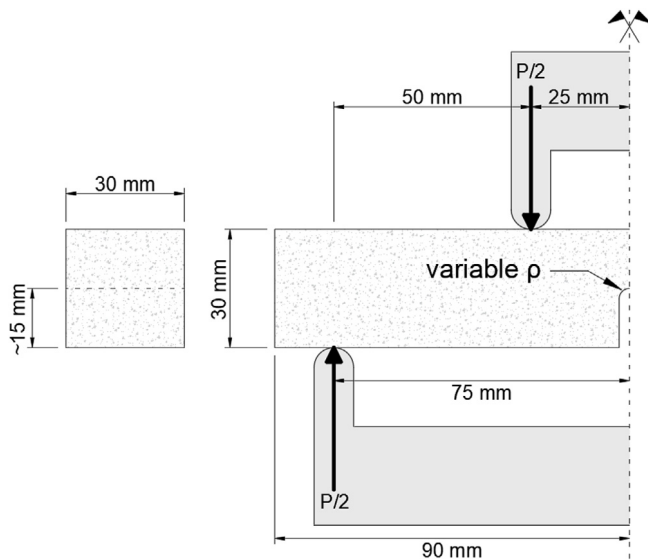


Fig. 4. Schematic representation of the SENB specimens subjected to Mode I loading conditions.

**Table 2**  
Some technical properties of the analysed rocks at room temperature.

	(F)	(C)	(M)	(I)
Bulk density ( $\text{kg/m}^3$ )	2320	2500	2715	2709
Open porosity (%)	16.3	6.4	–	–
Water absorption (%)	4.80	2.70	0.075	0.15
Mean grain size ( $\mu\text{m}$ )	116	218	335	142
Median grain size ( $\mu\text{m}$ )	109	183	282	131

tests (Fig. 3b) and four-point bending tests (Fig. 3c), which are described in the following subsections. This work uses the experimental data reported by the authors in a previous work,<sup>13</sup> where the TCD was used for the assessment of notched rock fracture at different temperatures. In particular, the experimental results of the four-point bending tests and tensile splitting tests at different temperatures studied in that work are recovered here and analysed using the SED criterion in this case. This approach requires some additional parameters such as the Young's modulus and the Poisson's ratio. Thus, the previous experimental campaign is extended in this work, performing several uniaxial compression tests at the same temperature conditions as those considered in the previous work.<sup>13</sup> Likewise, using the same strain gauge system as in the uniaxial compression tests, several thermal dilatation measurements have been taken in this work to compare with those measurements of the digital comparator provided in the previous laboratory campaign.<sup>13</sup>

All the tests have been carried out inside a heat chamber under displacement and temperature control. Therefore, constant temperature conditions are guaranteed throughout the duration of the tests. The chamber is coupled to the press in such a way that the loads are transferred to the testing devices through two steel shafts crossing the chamber walls. The upper shaft is provided with a spherical joint that allows a greater degree of adjustment while ensuring that the axis of load application remains centred. Besides, all the specimens were preheated to the target temperature for at least 48 h before testing. Thus, temperature within the specimens can be assumed to be constant and homogeneous during the tests according to Newton's heating law, which describes the change in temperature in an object and states that the heating rate is directly proportional to the difference in temperatures between the body and its surroundings.

### 3.2.1. Tensile splitting tests

In total, 144 tensile splitting tests (or Brazilian tests) have been performed using  $\text{Ø}64\text{mm}$  disc specimens (with a diameter/depth ratio of 2) and according to the ASTM standards.<sup>46</sup> More specifically, 6 tests were carried out for each rock and temperature, considering 23 °C (room temperature), 70 °C, 110 °C, 150 °C, 200 °C and 250 °C.

Although the Brazilian test is an indirect method, it is commonly used to obtain the tensile strength of rocks due to its simplicity.<sup>47</sup> The test procedure for those specimens at elevated temperatures was the same as for the room temperature case. Fig. 3a shows the standardised testing device with curved platens that was used for performing the Brazilian tests.

### 3.2.2. Uniaxial compression tests

120 uniaxial compression tests have been carried out using cylindrical specimens with 50 mm diameter and 150 mm height. The specimens were instrumented with special high temperature resistant strain gauges to measure both the longitudinal and diametrical deformations during loading, which allows the deformational parameters ( $E$ ,  $\nu$ ) of the rocks to be obtained from the stress–strain curves.

These tests were performed according to the European standards,<sup>48,49</sup> maintaining once again the same procedure for the tests at high temperatures. Four different temperatures were considered in this case: 23 °C, 70 °C, 150 °C and 250 °C. Fig. 3b shows the experimental set-up of the uniaxial compression tests, where a Wheatstone bridge circuit is created using a compensation rock sample inside the chamber subjected to no loads.

### 3.2.3. Four-point bending tests

Almost 800 four-point bending tests on SENB specimens have been performed altogether, 6 tests (or 12 in some cases for verification purposes) per rock type, temperature and notch radius combination. The geometry of the specimens and the loading mode is schematised in Fig. 4. The proposed configuration ensures a constant bending moment and no shear stresses between the inner loading points where the notches are located. Thus, Mode I loading conditions are fulfilled. On the other hand, fixed semi-circular supports have been used to perform the four-point bending tests (see Fig. 3c). Although rolling supports would be desirable according to Ayatollahi et al.<sup>50</sup> and Bahrami et al.<sup>51</sup>, friction effects between supports and specimens are considered to have a minor influence in this case because of the distance between supporting rollers (namely, 150 mm) and the small displacements prior to failure.

The tested specimens consist of parallelepiped  $180 \times 30 \times 30$  mm size SENB samples with notch radii ( $\rho$ ) of 0.15, 0.5, 1, 2, 4, 7, 10 and 15 mm and notch lengths of approximately half of the height, with slight variations caused by the precision of the cutting processes. The smallest notches, those with  $\rho$  equal to 0.15 and 0.5 mm, were manufactured using rotating diamond wires, while the rest of the notches were made using abrasive discs with semi-circular contour. In any case, both methods offer U-shaped notches, and the relative notch length ( $\alpha_0$ ), defined as the ratio between the real notch length and the total height of the specimen, has been limited to  $0.45 \leq \alpha_0 \leq 0.55$  to ensure high constraint conditions. Likewise, plane strain conditions have been assumed.

These tests were performed with a constant loading rate of 0.05 mm/min till failure, according to the Spanish<sup>52</sup> and European<sup>53</sup> standards. As in the former tests, all the four-point bending tests were executed inside the heat chamber at different temperature conditions. In this case, the selected temperatures were 23 °C, 70 °C, 150 °C and 250 °C.

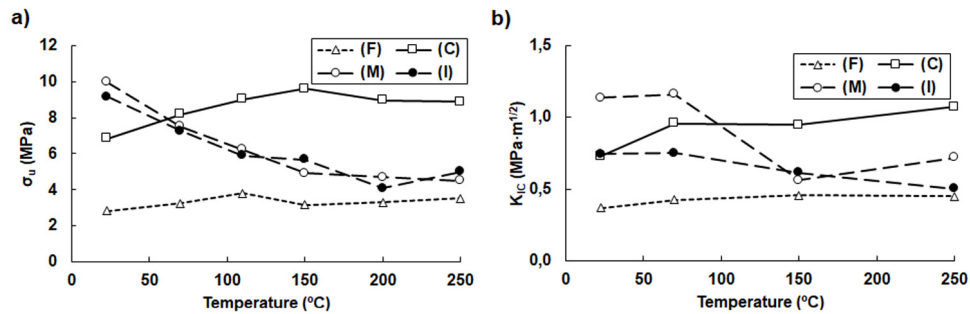


Fig. 5. Variation of the (a) tensile strength  $\sigma_u$  and (b) fracture toughness  $K_{IC}$  with temperature of the analysed rocks.

### 3.2.4. Thermal expansion measurements

As emphasised in previous comments, the differential thermal expansion of adjacent grains and their constraint conditions (the presence or lack of internal space for expansion) can define to a great extent the thermal damage and the mechanical behaviour of the rocks under different thermal conditions. For this reason, the dilatation curves of the four analysed rocks have been studied here in an attempt to distinguish different dilatation patterns. To this end, the thermal expansion was measured using two different methods. First, the longitudinal deformation of prismatic ( $180 \times 30 \times 30$  mm) rock samples was checked at different temperature steps by means of a digital comparator. Proceeding along similar tracks, the longitudinal and diametric deformation of cylindrical (50 mm diameter and 150 mm length) rock samples were measured using strain gauges and a piece of Invar36 as a compensation sample. Invar36 is a nickel–iron alloy that exhibits an almost zero rate of thermal expansion ( $\sim 10^{-6}$  mm/mm/°C) from cryogenic temperatures to approximately 260 °C, which makes it suitable for this analysis.

## 4. Results

### 4.1. Influence of temperature on tensile strength

A proper definition of the tensile strength ( $\sigma_u$ ) is very important for the correct application of the SED criterion, since the critical strain energy density ( $W_c$ ) and the value of  $R_c$  (which defines the control area) depend on the square of this parameter according to Eqs. (1) and (4), respectively.

Fig. 5a represents the variation with temperature of the tensile strength of the four analysed rocks. Only the mean values are represented for the sake of clarity, but the individual results of the tensile splitting tests are gathered in Appendix A.

Broadly speaking, two different trends can be distinguished from the curves in Fig. 5a, which are probably linked to the microstructure of each rock. Firstly, the Moleano limestone (C) undergoes an increment of  $\sigma_u$  up to a critical temperature (150 °C) and then slightly decreases. This behaviour pattern is similar to the one observed in the Floresta sandstone (F), although in this case the variation with temperature is less pronounced in relative terms. Both the limestone and the sandstone present a certain porosity as shown in Table 2, 6.4% and 16.3% respectively. Thus, the observed initial increment of the tensile strength could be explained by the partial closure of these pores (or other microfeatures) and the loss of ambient humidity. Then, the stresses generated by the differential thermal expansion of adjacent grains and the lack of space for further expansion lead to the appearance of new microcracks and, therefore, to a decrease of the tensile strength.

On the other hand, the two marbles studied present a considerably similar tendency of the tensile strength with temperature. They both reveal a clear reduction of  $\sigma_u$  from the onset of the

temperature increase. As displayed in Table 2, the Macael marble (M) and the Carrara marble (I) exhibit no significant porosity in their microstructure. For this reason, there is no space for the expansion of the mineral particles within the rock matrix and thermally induced microcracks appear when the temperature starts to rise.

Similar conclusions have been obtained by other authors<sup>8,9,54,55</sup> to explain the variation with temperature of the tensile strength of different (but comparable) rocks. For example, Rao et al.<sup>56</sup> reported the case of a sandstone where the tensile strength increased up to 250°C, after which it decreased. They related the observed increment to the compaction caused by the expansion of the grains, and they attributed the subsequent reduction of  $\sigma_u$  to the new pores and fissures created during the continuous expansion of the mineral particles. Other studies on the thermal behaviour of igneous rocks such as granites and basalts (e.g., Refs. 9, 55) showed that the tensile strength decreased with temperature and suggested that this was associated to the low porosity. Thus, the differential thermal expansion of nearby grains and the boundary conditions of those grains (e.g., presence of pores, cavities, microcracks) that allow or limit their expansion seem to define the thermal behaviour of the rocks at the macro-scale.

### 4.2. Influence of temperature on fracture toughness

Fracture toughness ( $K_{IC}$ ) represents the resistance to propagation of a cracked component, that is, the fracture energy consumption rate required to generate new surfaces along the crack. For this reason, the variation of  $K_{IC}$  with temperature is also deeply related to the microstructure of the analysed material, since the required fracture energy for the creation of new surfaces is reduced in the presence of thermally induced microcracks, which facilitate crack propagation especially under mode I loading conditions (opening case). The opposite situation may also occur, as the fracture toughness could increase with the closure of pores or pre-existing microcracks, similarly to the case of the tensile strength.

By definition, the fracture toughness corresponds to a cracked situation with a notch radius ( $\rho$ ) equal to zero. However, as demonstrated by the authors in a previous work<sup>22</sup> for a number of rocks, when the notch radius is sufficiently small the notch effect is negligible. Thus, those SENB samples with the smallest notch radius ( $\rho = 0.15$  mm) have been assumed to behave as crack-type defects, and therefore, the obtained  $K_{IC}$  value is equal to the one corresponding to a real crack ( $\rho = 0$  mm).

Srawley and Gross<sup>57</sup> proposed the following expression for the calculation of the stress intensity factor ( $K_I$ ) of SENB specimens:

$$K_I = \frac{P \cdot Y}{b \cdot h^{1/2}} \quad (6)$$

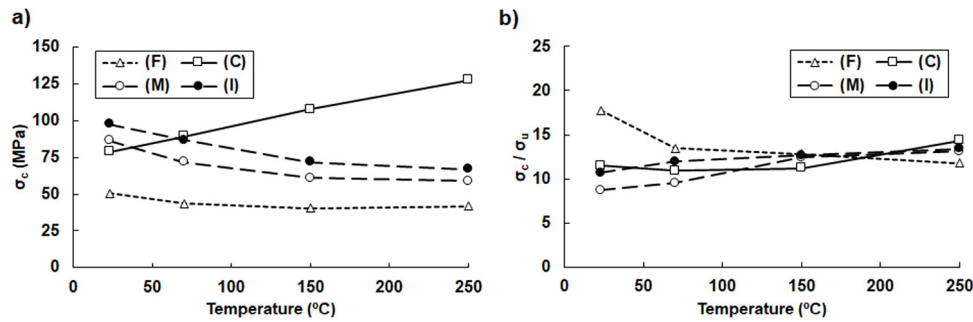


Fig. 6. Variation of the (a) uniaxial compressive strength  $\sigma_c$  and (b)  $\sigma_c/\sigma_u$  ratio with temperature of the analysed rocks.

Table 3

Mean values and standard deviation of the uniaxial compression strength (in MPa) of each of the analysed rocks at different temperatures. F: Floresta sandstone; C: Moleano limestone; M: Macael marble; I: Carrara marble.

	(F)		(C)		(M)		(I)	
	Mean	S. Dev.	Mean	S. Dev.	Mean	S. Dev.	Mean	S. Dev.
23 °C	50.44	2.58	78.75	8.10	86.63	8.81	97.80	4.45
70 °C	43.79	4.37	89.27	8.84	71.79	5.26	86.85	5.71
150 °C	40.61	6.10	107.75	21.61	61.12	5.47	71.87	3.26
250 °C	41.72	6.90	127.54	17.15	59.00	4.60	67.01	3.92

where  $P$  is the applied load,  $b$  and  $h$  are the depth and height of the samples, both of them equal to 30 mm according to Fig. 4, and  $Y$  is a non-dimensional geometrical factor given by:

$$Y = \frac{3(L_o - L_i) \cdot \alpha_0^{1/2} \cdot X}{2h \cdot (1 - \alpha_0)^{3/2}} \quad (7)$$

with

$$X = 1.9887 - \left[ \frac{(3.49 - 0.68\alpha_0 - 1.35\alpha_0^2) \cdot \alpha_0 \cdot (1 - \alpha_0)}{(1 + \alpha_0)^2} \right] - 1.32\alpha_0 \quad (8)$$

$L_o$  is equal to the span between the outer supporting rollers (150 mm),  $L_i$  is the distance between the inner loading points (50 mm) and  $\alpha_0$  is the relative notch length of each particular sample.

According to traditional linear-elastic fracture mechanics for the analysis of cracks, when the stress intensity factor reaches the fracture toughness ( $K_I = K_{IC}$ ) failure occurs. In that situation, the load  $P$  in Eq. (6) corresponds to the failure load. Therefore, the fracture toughness can be calculated by inverting that expression and considering the failure load obtained in the four-point bending tests for the specimens with  $\rho = 0.15$  mm.

With all this, the curves in Fig. 5b represent the variation of  $K_{IC}$  with temperature for each of the analysed rocks. These results correspond to the mean values of the fracture toughness. The individual results of  $K_{IC}$  have also been included in Appendix A.

Both the Floresta sandstone (F) and the Moleano limestone (C) show a continuous increment of the fracture toughness from the onset of the temperature increment, although this increase is somewhat less pronounced in the sandstone in relative terms. As in the case of the tensile strength, this growth tendency should be limited by a critical temperature. However, the temperature after which the fracture toughness decreases for these particular rocks seems to be higher than the studied range of temperatures. On the other hand, both marbles show no significant variation of  $K_{IC}$  in the increment step up to 70 °C. Then, an important drop of the fracture toughness is observed.

The comments on the reasons explaining the observed tendencies in the tensile strength with temperature are also attributable to the fracture toughness. For example, Mahanta et al.<sup>58</sup> studied

the influence of temperature on the fracture toughness of two types of sandstones and a dolomite and used scanning electron microscope (SEM) analyses to measure the microcracks that were induced within those rocks as a result of the thermal treatment. They reported an increment of the fracture toughness of the three rocks up to approximately 100 °C and ascribed it to the closure of pre-existing cracks and to the desorption of the water that was present in those rocks. Then, they observed a gradual fall in the fracture toughness up to 600°C, caused by thermally induced new microcracks, which were clearly visible (from SEM and petrographic thin-section analyses) for temperatures higher than 200 °C.

#### 4.3. Influence of temperature on uniaxial compressive strength

The variation of the uniaxial compressive strength ( $\sigma_c$ ) with temperature is analysed in this subsection. This parameter has no influence on the application of the SED criterion, but it provides a better characterisation of the studied rocks and the uniaxial compression tests were necessary to obtain the deformational parameters. Table 3 gathers the mean values and the standard deviation of  $\sigma_u$  for each of the analysed rocks and temperatures, and the individual results are collected in Appendix A.

The obtained mean values of the compressive strength are plotted in Fig. 6a to observe trends more clearly. The Floresta sandstone (F) develops a slight decrease of the compressive strength when temperature increases. Both marbles (M and I) show a similar pattern to the sandstone but the decrease is more pronounced in relative terms. In contrast to the previous rocks, an important increment of the compressive strength of the Moleano limestone (C) is appreciated up to 250 °C. Fig. 6b represents the ratio between the compressive and the tensile strength of the rocks with temperature. Both marbles and the limestone present a slight increment of the  $\sigma_c/\sigma_u$  with temperature, while the sandstone reveals a significant drop from 23 °C to 70 °C and a successive slight decrement for higher temperatures up to 250 °C. In general, a roughly constant evolution of  $\sigma_c/\sigma_u$  could be interpreted from Fig. 6b, except for the first temperature step of the Floresta sandstone (F), which means that both the compressive and the tensile strength of each rock vary more or less proportionally with temperature.

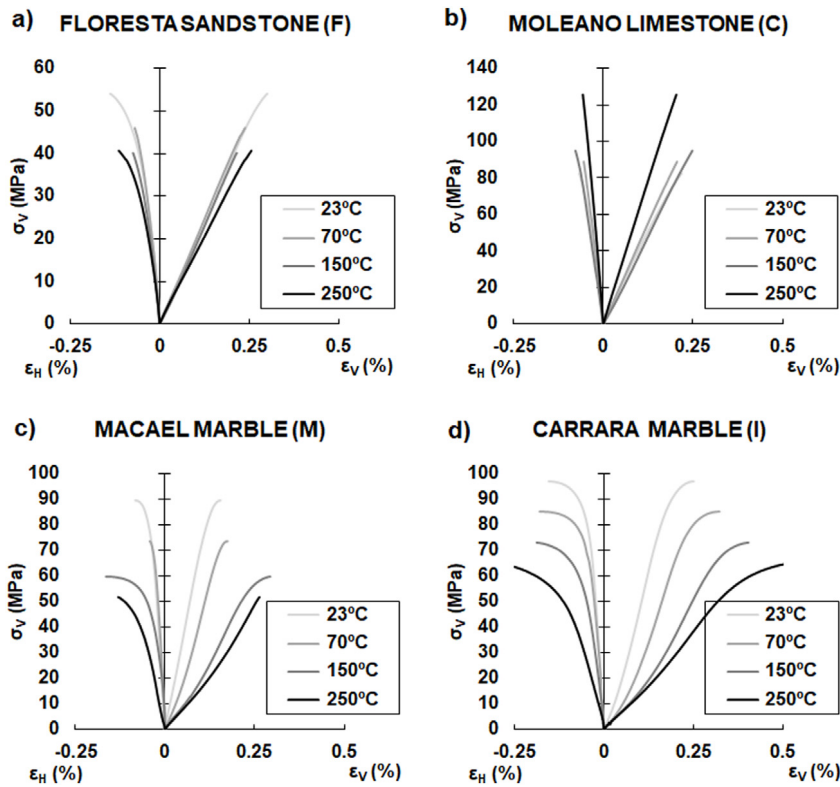


Fig. 7. Representative stress–strain curves of the uniaxial compression tests at different temperatures.

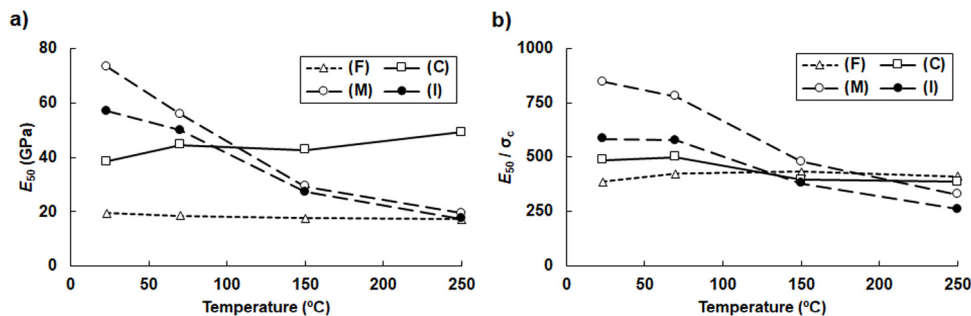


Fig. 8. Variation of the (a) Young's modulus  $E_{50}$  and (b)  $E_{50}/\sigma_c$  ratio with temperature of the analysed rock.

Several papers can be found in the literature on the performance of uniaxial compression tests on rocks under different temperature conditions. In most of the cases, the rock strength and deformation modulus decrease with increasing temperature, especially beyond a certain temperature (e.g., Refs. 55, 59). Yang et al.<sup>21</sup> for example, investigated the strength and thermal cracking of granite under uniaxial compression using thin section and X-ray micro computed tomography. Their experimental results showed that the tested granite strengthened at 300 °C, and weakened above 300 °C. Tullis and Yund<sup>60</sup> also reported uniaxial compression test results of a granite and showed that both the uniaxial compressive strength and the Young's modulus decreased with increasing temperature.

#### 4.4. Influence of temperature on Young's modulus and Poisson's ratio

From the deformational measurements of the uniaxial compression tests the Young's modulus ( $E$ ) and the Poisson's ratio

( $\nu$ ) of the rocks have been derived at room temperature and at higher temperatures up to 250 °C. The strain energy ( $W$ ) depends on both parameters as deduced from Eq. (2) for an isotropic and linear elastic material. For this reason, the study of the variation of  $E$  and  $\nu$  with temperature provides valuable information on the influence of temperature on the strain energy.

In order to verify whether or not the use of Linear Elastic Fracture Mechanics (LEFM) is valid up to 250 °C, the stress–strain curves are presented in Fig. 7. The linearity of the curves prior to the peaks reveals a predominantly quasi-brittle behaviour of the Floresta sandstone (F) and the Moleano limestone (C) in the entire range of temperatures considered in this work (Figs. 7a and 7b). By contrast, the influence of temperature on the linear elastic behaviour of the marbles (Figs. 7c and 7d) is more significant, especially in the Carrara marble (I). Both marbles show a certain degree of ductility in relative terms, which seems to be more noticeable as temperature increases. In the case of the Macael marble (M), reasonable brittle behaviour is observed at

**Table 4**

Mean values and standard deviation of the Young's modulus (in GPa) of each of the analysed rocks at different temperatures. F: Floresta sandstone; C: Moleano limestone; M: Macael marble; I: Carrara marble.

	(F)		(C)		(M)		(I)	
	Mean	S. Dev.						
23 °C	19.52	1.98	38.40	4.74	73.41	7.11	57.13	3.73
70 °C	18.52	1.24	44.60	2.20	55.90	6.59	50.05	2.77
150 °C	17.58	2.28	42.73	9.37	29.37	4.88	27.35	3.07
250 °C	17.23	2.05	49.22	15.88	19.42	3.07	17.43	1.44

**Table 5**

Mean values and standard deviation of the Poisson's ratio of each of the analysed rocks at different temperatures. F: Floresta sandstone; C: Moleano limestone; M: Macael marble; I: Carrara marble.

	(F)		(C)		(M)		(I)	
	Mean	S. Dev.						
23 °C	0.359	0.040	0.312	0.051	0.349	0.064	0.351	0.035
70 °C	0.293	0.048	0.275	0.014	0.277	0.039	0.297	0.048
150 °C	0.321	0.017	0.282	0.024	0.354	0.073	0.310	0.029
250 °C	0.335	0.037	0.282	0.051	0.421	0.139	0.468	0.085

**Table 6**

Critical length ( $R_c$ ) and critical strain energy ( $W_c$ ) of each rock and temperature. F: Floresta sandstone; C: Moleano limestone; M: Macael marble; I: Carrara marble.

	TEMP. (°C)	$R_c$ (mm)	$W_c$ (KPa)
(F)	23	3.9049	0.2066
	70	4.7813	0.2852
	150	5.3828	0.2858
	250	3.9564	0.3656
(C)	23	2.9638	0.6128
	70	3.9156	0.7501
	150	2.7321	1.0828
	250	4.0653	0.8011
(M)	23	3.1008	0.6770
	70	6.7355	0.5058
	150	3.1330	0.4121
	250	4.7303	0.5215
(I)	23	1.5380	0.7344
	70	2.8892	0.5265
	150	3.1413	0.5877
	250	1.4685	0.7170

23 °C and 70 °C, but a certain non-linearity is noticed for higher temperatures. In the case of the Carrara marble (I), however, even those tests performed at room temperature display a not completely linear behaviour (e.g., Fig. 7d at 23 °C). Regardless of these comments, the four studied rocks have been assumed to behave as quasi-brittle materials and the explained methodology (based on the linear-elastic formulation of the SED criterion) has been applied in all the cases. With this in mind, worse fracture load predictions should be expected as non-linear behaviour becomes more significant.

Comparing the obtained results with data in the literature, a certain degree of plasticity has been observed in other studies at temperatures of around 100 °C in the case of marbles (e.g., Ref. 15), between 250 °C and 500 °C for studies on sandstones (e.g., Refs. 15, 56) and 700 °C on limestones (e.g., Ref. 61).

Tables 4 and 5 collect, respectively, the experimentally obtained mean values and the standard deviation of the Young's moduli and Poisson's ratios. Likewise, the individual test results are compiled in Appendix A. The values of  $E$  obtained correspond to the tangent Young's modulus at a stress level equal to 50% of the ultimate uniaxial compressive strength ( $E_{50}$ ). Similarly, the Poisson's ratio values have been calculated in the same manner

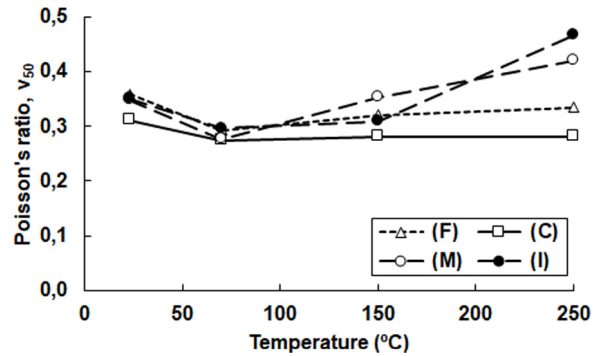


**Fig. 9.** Variation of the Poisson's ratio ( $v_{50}$ ) with temperature of the analysed rocks.

considering the tangent slopes of the axial and diametric stress-strain curves (Fig. 7) at 50% of the peak strength ( $v_{50}$ ), following the ISRM recommendations.<sup>62</sup>

The variation of the mean Young's modulus with temperature is represented in Fig. 8a for each of the analysed rocks. The slope of the Floresta sandstone's (F) curve is slightly decreasing (practically constant), which means that the influence of temperature on the Young's modulus is almost negligible at least up to 250 °C, similar to the trend observed in the compressive strength. The Macael marble (M) and the Carrara marble (I) offer a similar thermal behaviour. They both reveal a clear reduction of the Young's modulus with temperature, although the Macael marble (M) provides slightly higher values of  $E$  in absolute terms. Finally, the Moleano limestone (C) shows a significant increment of the Young's modulus with temperature, although the growth is gentler than that observed in Fig. 6a for the compressive strength in relative terms.

Fig. 8b represents the ratio between the Young's modulus and the compressive strength of the rocks. The Floresta sandstone (F) and the Moleano limestone (C) show an approximately constant ratio with temperature. Thus, the variation of the Young's moduli and the compressive strengths are proportional as temperature increases. However, the Macael marble (M) and the Carrara marble (I) display a significant reduction of  $E_{50}/\sigma_c$  with temperature. This involves a relatively higher decrease of  $E_{50}$  with temperature compared to the decrease of  $\sigma_c$ . These conclusions are consistent with the stress-strain curves in Fig. 7. In fact, the observed strains

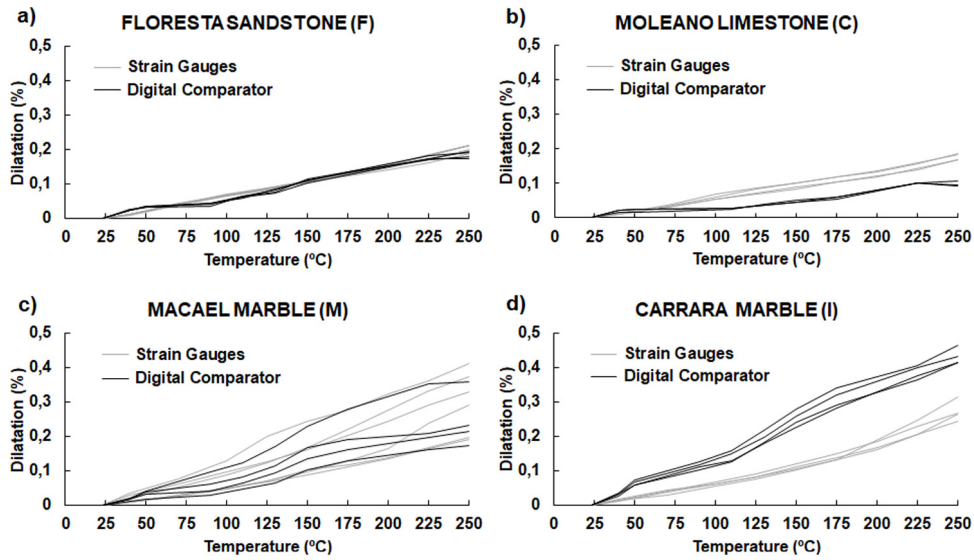


Fig. 10. Thermal dilatation measurements of the analysed rocks using strain gauges and a digital comparator.

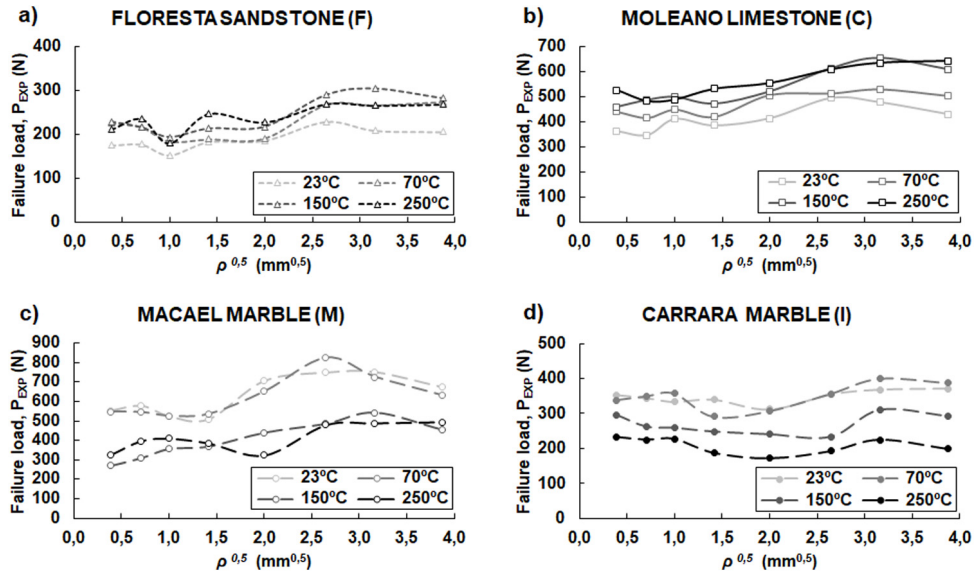


Fig. 11. Mean failure loads of the four-point bending tests for each rock and temperature.

for 50% of the compressive strength are roughly constant in the case of the Floresta sandstone (F) and the Moleano limestone (C), which could explain the slight variations of  $E_{50}/\sigma_c$  with temperature. However, in the case of the Macael marble (M) and the Carrara marble (I), those same strains increase with temperature and, therefore, it could be concluded that  $E_{50}/\sigma_c$  decreases as temperature gets higher because of the non-linearities of these rocks.

In the same way, Fig. 9 represents the variation of the average Poisson's ratio in the considered range of temperatures up to 250 °C. The four analysed rocks suggest a reduction of the Poisson's ratio up to approximately 70 °C. Then, both the Floresta sandstone (F) and the Moleano limestone (C) show a roughly constant value of around 0.3 up to 250 °C, while the marbles present a clear and relatively steep increment. The high values approaching 0.5 for 250 °C are attributable to the lack of linear elastic behaviour of the marbles at that temperature, especially in

the Carrara marble (I). It is also worth noting that  $v_{50}$  (obtained in a consistent way with  $E_{50}$ ) is higher than for example  $v_0$ , which considers the initial slope of the strain curves.

#### 4.5. Thermal expansion

Fig. 10 compares the obtained thermal dilatation measurements (in percentage) for each of the analysed rocks and described methods. In all the cases, the noted dilatation readings are relative to the prior temperature steps. Analysing the curves, it is complicated to obtain clear and generalisable conclusions. However, several observations should be highlighted. Firstly, the two measurement methods offer similar results in the case of the Floresta sandstone (F) and the Macael marble (M), but present significant differences in the Moleano limestone (C) and the Carrara marble (I). Secondly, both marbles reveal the largest scatter

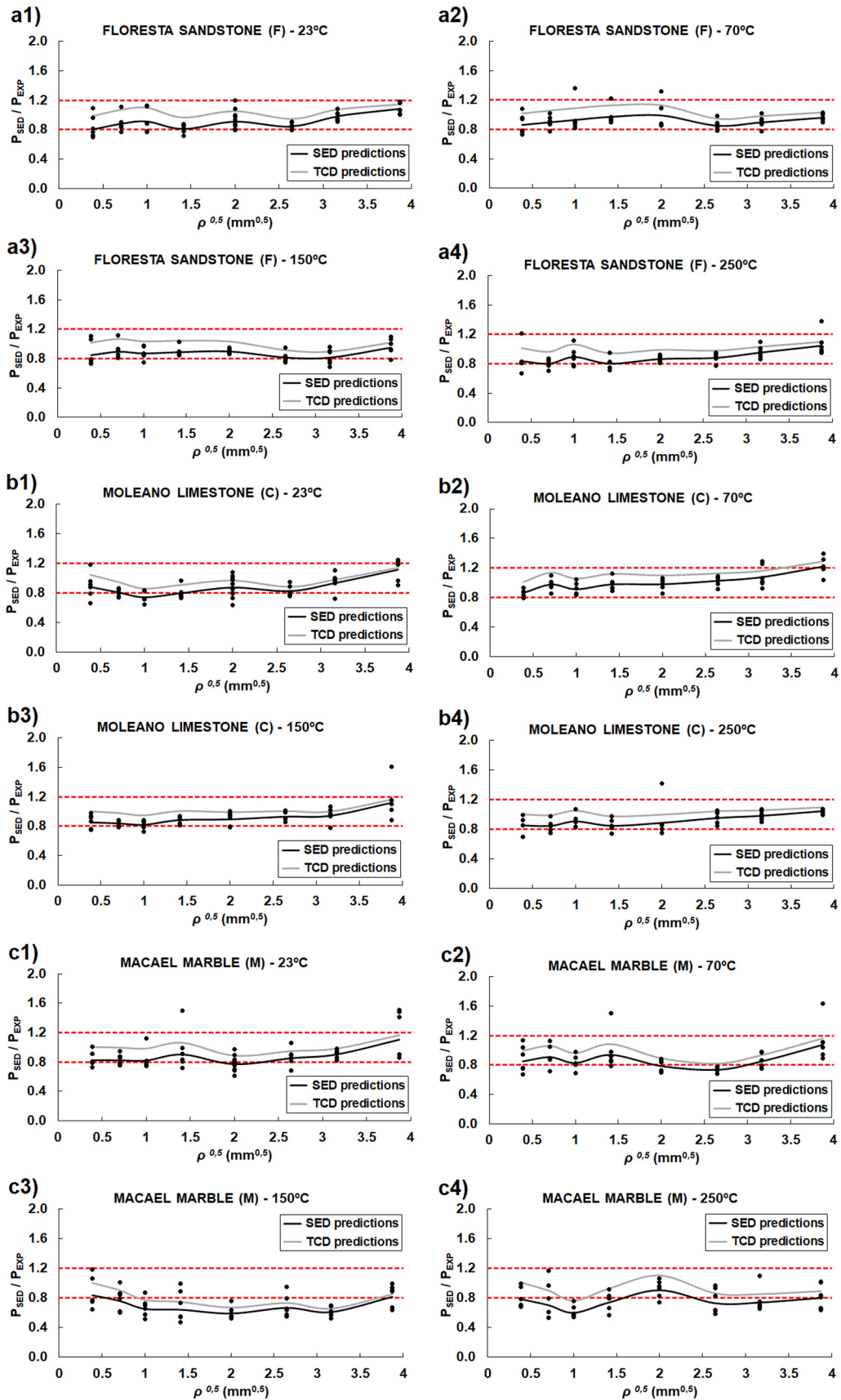


Fig. 12. Failure load predictions according to the SED criterion for each rock and temperature, and comparison with TCD results.<sup>13</sup>

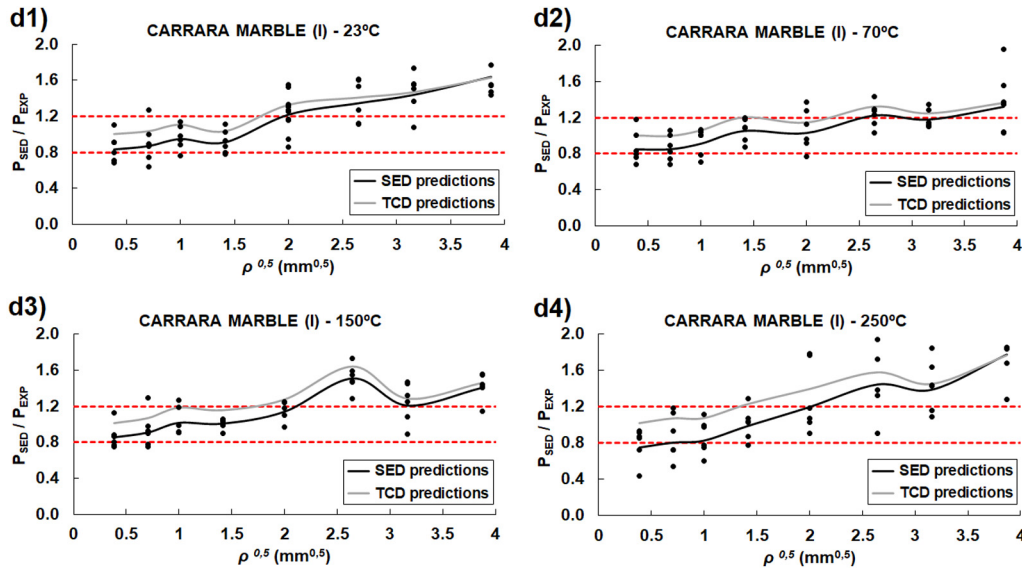


Fig. 12. (continued).

of the results, regardless of the measuring method as shown in Fig. 10c for the case of the Macael marble (M).

It is also important to take into account that the dilatation values are provided as a percentage. However, the digital comparator readings correspond to the elongation of the whole specimen in the longitudinal dimension (180 mm), while the strain gauges are measuring deformations within a representative surface covered by the electrical resistor, which is 6 mm in length. These strain gauges are more than ten times larger than the mean grain size of the rocks (Table 2), as required by the standards.<sup>49</sup>

In this sense, analysing the digital comparator curves of the Floresta sandstone (F) and the Moleano limestone (C) in Figs. 10a and 10b, a quasi-horizontal zone can be distinguished in the slopes from approximately 50 °C to around 90 °C in the case of the sandstone and 110 °C in the limestone. These regions, which are only appreciated in the porous rocks, could entail no significant external dilatation of the samples. Thus, they could be governed by the inner expansion where the pre-existing pores, cavities or microcracks get closed. This phenomenon is obviously limited and after reaching a critical temperature, the mechanism changes and external dilatation seems to be dominant. By contrast, both marbles show significant external dilatation from the onset of heating, which agrees with their null porosity and the damage induced by differential thermal dilatation.

#### 4.6. Bending tests with different notch radii and different temperatures

Fig. 11 gathers the experimentally obtained mean failure loads ( $P_{EXP}$ ) of the four-point bending tests for each rock, temperature and notch radius. In general terms, the failure load seems to increase with temperature in the case of the porous rocks (Figs. 11a and 11b) and decreases in the case of the non-porous marbles. These trends are consistent with those comments made in Section 4.1 on the thermal dilatation of adjacent grains with or without internal space for expansion. Likewise,  $P_{EXP}$  also shows a growing trend with the notch radius. This statement is logical, since notches with large radii develop smaller stress concentrations at the notch tip than those with a small radius. However, this generality is not reflected so clearly in the case of the Carrara marble (I) at high temperatures, probably because this rock does not behave as a linear elastic material at those temperatures (Fig. 7d).

## 5. Fracture assessment

### 5.1. Methodology

According to the failure criterion defined by the SED approach ( $\bar{W} = W_c$ ), the analysis of fracture processes in notched components can be made by a direct comparison of the critical value of the strain energy density provided by Eq. (1) with the average SED within the control area ( $\Omega$ ) provided by Eq. (5). Thus, the failure conditions are met when the following expression is fulfilled<sup>30</sup>:

$$W_c = 0.785 \cdot H \left( v, \frac{R_c}{\rho} \right) \cdot \frac{\sigma_{max}^2}{E} \quad (9)$$

The maximum stress at the notch tip ( $\sigma_{max}$ ) corresponds to the failure situation. Therefore, the failure load can be derived from such stress conditions. Here, this is done by means of the stress-distribution function at the notch tip proposed by Creager and Paris<sup>53</sup>:

$$\sigma(r) = \frac{K_I}{\sqrt{\pi}} \frac{2(r + \rho)}{(2r + \rho)^{3/2}} \quad (10)$$

$K_I$  being the stress intensity factor of a crack with the same dimensions of the notch being analysed,  $\rho$  being the notch radius and  $r$  the distance from the notch tip. The stress will be maximum for  $r = 0$  mm. Thus:

$$\sigma_{max} = \sigma(r = 0) = \frac{2K_I}{\sqrt{\pi\rho}} \quad (11)$$

With all this, considering the energy-based failure criterion established by Eq. (9), the maximum stress at the notch tip defined in Eqs. (11) and (6) defining  $K_I$  for the particular case of SENB specimens, the predicted failure load (here referred to as  $P_{SED}$ ) can be calculated. The resulting expression is:

$$P_{SED} = \frac{b}{2Y} \sqrt{\frac{W_c \cdot E \cdot \rho \cdot \pi \cdot h}{0.785 \cdot H}} \quad (12)$$

$b$ ,  $h$  and  $\rho$  are previously defined geometrical parameters,  $Y$  is the non-dimensional factor defined in Eq. (7), which also depends on geometrical aspects, and  $E$  is the Young's modulus. The critical strain energy ( $W_c$ ) has been assumed to be constant for each rock and temperature, presuming that the analysed rocks behave as linear-elastic materials at the studied range of temperatures. Under this hypothesis,  $W_c$  is calculated using Eq. (1). Finally, the

**Table 7**  
Extrapolated values of the  $H$  function for U-notched specimens.

$R_c/\rho$	$\nu = 0.10$	$\nu = 0.15$	$\nu = 0.20$	$\nu = 0.25$	$\nu = 0.30$	$\nu = 0.35$	$\nu = 0.40$	$\nu = 0.45$
0.0005	0.6294	0.6215	0.6104	0.5960	0.5785	<b>0.5577</b>	<b>0.5337</b>	<b>0.5065</b>
0.001	0.6286	0.6207	0.6095	0.5952	0.5777	<b>0.5571</b>	<b>0.5332</b>	<b>0.5061</b>
0.005	0.6225	0.6145	0.6033	0.5889	0.5714	<b>0.5506</b>	<b>0.5268</b>	<b>0.4997</b>
0.01	0.6149	0.6068	0.5956	0.5813	0.5638	0.5432	0.5194	<b>0.4925</b>
0.05	0.5599	0.5515	0.5401	0.5258	0.5086	0.4884	0.4652	<b>0.4392</b>
0.1	0.5028	0.4942	0.4828	0.4687	0.4518	0.4322	0.4099	<b>0.3848</b>
0.3	0.3528	0.3445	0.3341	0.3216	0.3069	0.2902	0.2713	<b>0.2503</b>
0.5	0.2672	0.2599	0.2508	0.2401	0.2276	0.2135	0.1976	<b>0.1801</b>
1	0.1590	0.1537	0.1473	0.1399	0.1314	0.1217	0.1110	<b>0.0992</b>
2	<b>0.0982</b>	<b>0.0950</b>	<b>0.0911</b>	<b>0.0866</b>	<b>0.0815</b>	<b>0.0758</b>	<b>0.0696</b>	<b>0.0629</b>
5	<b>0.0433</b>	<b>0.0418</b>	<b>0.0400</b>	<b>0.0379</b>	<b>0.0356</b>	<b>0.0330</b>	<b>0.0302</b>	<b>0.0272</b>
10	<b>0.0224</b>	<b>0.0216</b>	<b>0.0207</b>	<b>0.0196</b>	<b>0.0184</b>	<b>0.0170</b>	<b>0.0155</b>	<b>0.0140</b>
20	<b>0.0114</b>	<b>0.0110</b>	<b>0.0105</b>	<b>0.0100</b>	<b>0.0093</b>	<b>0.0086</b>	<b>0.0079</b>	<b>0.0071</b>
30	<b>0.0077</b>	<b>0.0074</b>	<b>0.0070</b>	<b>0.0067</b>	<b>0.0062</b>	<b>0.0058</b>	<b>0.0053</b>	<b>0.0047</b>
40	<b>0.0058</b>	<b>0.0056</b>	<b>0.0053</b>	<b>0.0050</b>	<b>0.0047</b>	<b>0.0044</b>	<b>0.0040</b>	<b>0.0036</b>
50	<b>0.0046</b>	<b>0.0044</b>	<b>0.0042</b>	<b>0.0040</b>	<b>0.0038</b>	<b>0.0035</b>	<b>0.0032</b>	<b>0.0029</b>

function  $H$  depends on  $\nu$  and  $R_c/\rho$ . Both  $\nu$  and  $\rho$  are already known parameters and  $R_c$  is calculated according to Eq. (4). Table 6 contains the calculated values of  $R_c$  and  $W_c$  of each of the analysed rocks and considered temperatures.

Once all the parameters have been defined, the only issue is how to obtain the  $H$  function. In a previous work, the authors<sup>42</sup> already applied the SED criterion for the fracture assessment of rocks at room temperature, and three different methodologies were proposed based on the direct use of Eq. (5). As mentioned in Section 2, the  $R_c$  values are relatively high in the case of rocks compared to other materials like steels or polymers. For this reason, the three suggested approaches<sup>42</sup> aimed to adapt the  $H$  function values to the required range of  $R_c/\rho$ . The first method directly applied existing tabulated values of  $H$  (as those collected in Table 1) and the corresponding extrapolations when necessary, avoiding the use of numerical modelling. By contrast, the other two methods were based on the numerical evaluation of the  $H$  function and  $W$ , respectively. In general terms, the fracture load predictions provided by the first and simplest method were accurate enough, and the improvement offered by the other methods based on numerical analyses did not justify the significant increase of the workload. Thus, the most straightforward method will be applied here for the fracture assessment of the analysed rocks at different temperatures; that is, tabulated values of  $H$  will be directly used.

Basically, the  $H$  values from Table 1 were used as a basis to obtain new data for larger combinations of  $R_c/\rho$  and  $\nu$  values. This was done by means of a double extrapolation, considering a second order polynomial function to extend the Poisson's ratio values and a first order rational function for larger ratios of  $R_c/\rho$ .<sup>42</sup> Further details of the extrapolation criteria are summarised in Appendix B.

With all this, Table 7 extends those  $H$  values collected in Table 1 (indicated in grey) for a broader range of  $R_c/\rho$  and  $\nu$  values (indicated in black). This new table is suitable for geomaterials like rocks where the critical length ( $R_c$ ) values are relatively high. Once the  $H$  is known, the failure assessments can be easily accomplished by applying Eq. (12).

### 5.2. Failure load predictions

In this section, the failure load predictions of the SENB specimens is assessed using the previously described methodology. Fig. 12 illustrates the obtained failure load predictions for each rock and temperature according to the SED criterion (black solid lines). The dots correspond to each of the individual results and

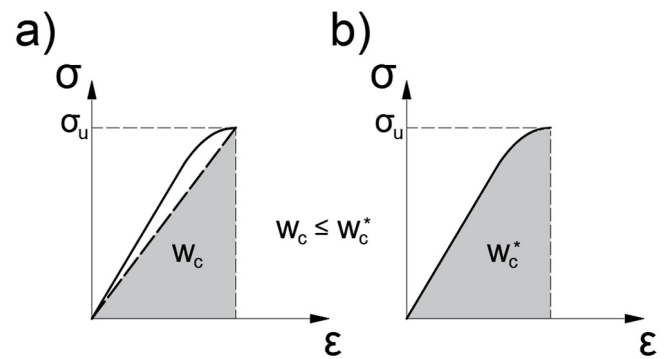


**Fig. 13.** Critical strain energy density calculated for (a) a theoretical linear behaviour ( $W_c$ ) or (b) for a non-linear behaviour ( $W_c^*$ ).

the solid line represents the mean failure predictions. For comparison purposes, the grey solid lines stand for the failure load predictions obtained by the authors in a previous work,<sup>13</sup> in which the TCD was used for the fracture assessment instead of the SED criterion. The vertical axis indicates the ratio between the predicted failure load ( $P_{SED}$ ) calculated with Eq. (12) and the experimentally obtained failure load ( $P_{EXP}$ ). Thus,  $P_{SED}/P_{EXP} = 1$  corresponds to the theoretical exact prediction, and the values below and above 1 imply underestimations and overestimations of the results, respectively. In the horizontal axis the square root of the notch radius ( $\rho^{0.5}$ ) has been represented in order to offer a clearer visualisation of the results corresponding to the smallest notches. Additionally, a band of  $\pm 20\%$  has been included in the graphs (horizontal dotted lines) as a criterion of accuracy, which is a common practice in fracture mechanics. This envelope aims to comprise the intrinsic uncertainties of the performed laboratory tests as well as the variability of the fracture results due to the heterogeneous nature of the rocks.

Several observations should be highlighted from the analysis of the results in Fig. 12. Both the Floresta sandstone (F) and the Moleano limestone (C), those rocks with the most evident linear-elastic behaviour (Fig. 7), offer relatively good failure predictions for the whole range of analysed temperatures (Figs. 12a and 12b). Similarly, the mean fracture prediction curves of the Macael marble (M) at 23 °C (Fig. 12c1) and at 70 °C (Fig. 12c2) also fall significantly within the defined  $\pm 20\%$  band. However, the results for 150 °C (Fig. 12c3) and 250 °C (Fig. 12c4) indicate a generalised underestimation. The stress-strain curves of the uniaxial compression tests for the Macael marble (M) at 150 °C

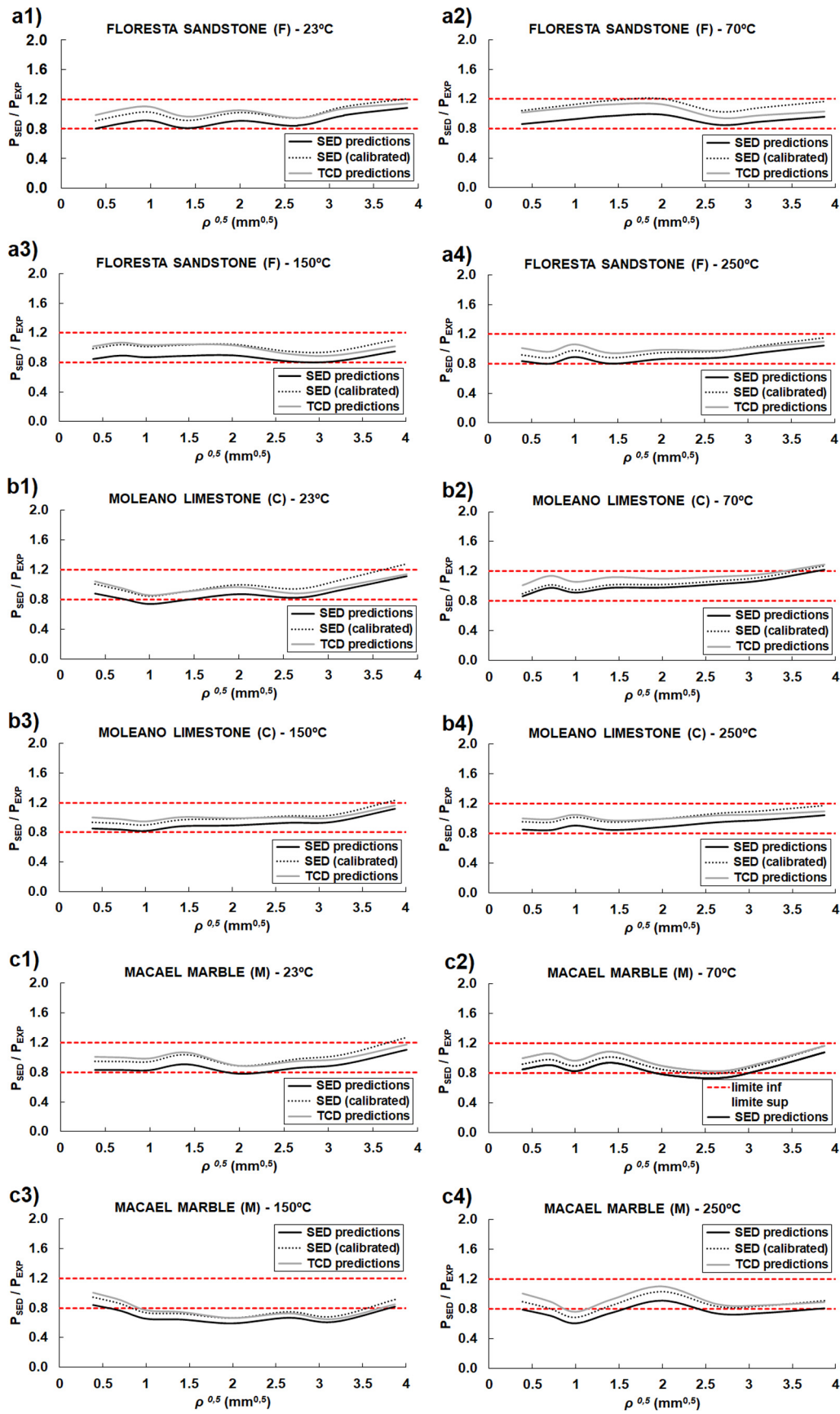


Fig. 14. Failure load predictions according to the SED criterion for each rock and temperature (both using the calculated values of  $W_c$  or the calibrated values of  $W_c^*$ ) and comparison with TCD results.<sup>13</sup>

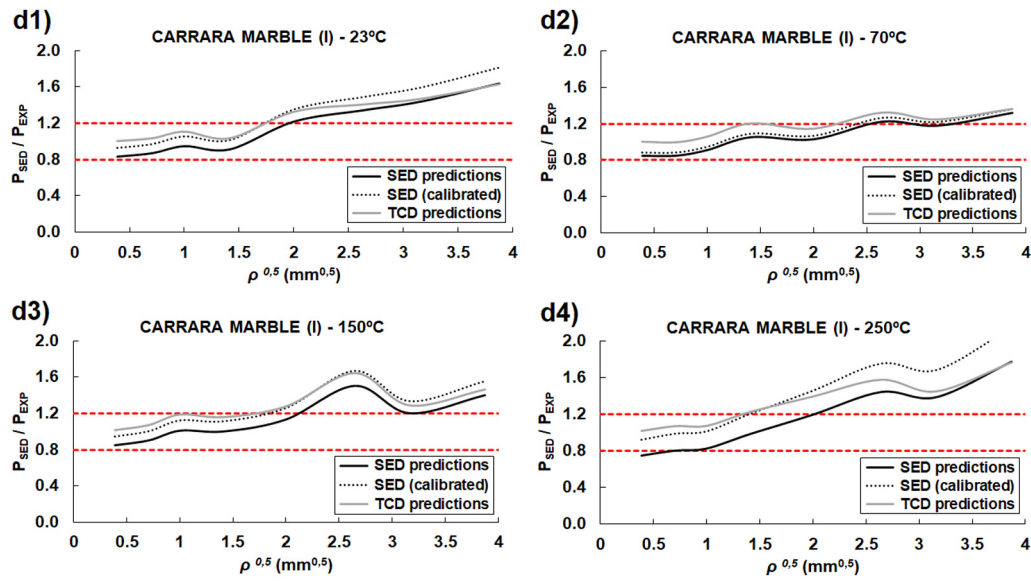


Fig. 14. (continued).

and 250 °C (Fig. 7c) suggest a not so linear behaviour at these temperatures, which could explain the worsening of the prediction shown in these two particular cases. The same argument could be attributed to the Carrara marble (I), the rock presenting the highest non-linearity in relative terms both at room and at higher temperatures (Fig. 7d). Besides, the stress field at the notch tip is defined by Eq. (10)<sup>63</sup> in this work, which is theoretically only valid for long and narrow notches. This could also affect the worsening of the failure predictions in the case of the largest notches, as in the case of the Carrara marble (I) for example. Despite this, relatively good failure predictions (within a  $\pm 20\%$  range) were obtained in the rest of the rocks even for the largest notches, although a general upward trend of  $P_{SED}/P_{EXP}$  is observed in many cases as the notches get larger (e.g., Fig. 12a1–c2).

Although both the TCD and the SED criterion offer relatively similar and accurate failure load predictions, certain differences are clearly observed. The SED criterion provides lower failure load predictions than the TCD in all the studied cases. This difference is more notorious in the case of the smallest notches and tends to reduce as the notch radius gets larger.

It is also important to remark that the represented SED failure predictions are calculated using the critical strain energy density value according to Eq. (1). Thus, this value corresponds to the theoretical area under a tensile test stress–strain curve assuming a strict linear behaviour till failure, as indicated in Fig. 13a. However, based on Fig. 7, certain subcritical crack growth prior to final failure can be expected, particularly at high temperatures. This leads to a non-perfectly linear behaviour as that indicated in Fig. 13b. The critical strain energy density corresponding to the area under the real non-linear stress–strain curve ( $W_c^*$ ) is larger than the calculated  $W_c$  value. Thus,  $W_c^*$  will provide higher load fracture predictions than  $W_c$ . The tensile stress–strain curves are not available in this work and are difficult to be obtained in rocks. As a simple approach to consider the material non-linearity in the estimation of  $W_c^*$ , its value can be calibrated for a particular notch radius and then be used for the failure load predictions of the rest of notch radii, since  $W_c^*$  is a material parameter. By just inverting Eq. (12) and leaving the critical strain energy density as the only unknown,  $W_c^*$  can be calibrated. In this work, for example,  $W_c^*$  has been calculated from the experimental failure load of the samples with  $\rho = 0.15$  mm. Accordingly, Fig. 14 represents, together with the TCD and SED load failure predictions depicted in Fig. 12,

black dotted curves with the new SED predictions based on the calibrated value of  $W_c^*$ . In general, the three methods (i.e., SED criterion, calibrated SED criterion and the TCD) provide relatively similar failure load estimations. It is observed that the calibrated SED failure predictions offer slightly higher estimations of the failure load (closer to  $P_{SED}/P_{EXP} = 1$  in many cases) providing, in general terms, similar results to those offered by the TCD. This calibration process can be applied in those cases in which non-linearities are not excessively large. However, when non-linear behaviour is important, the SED criterion can no longer be applied as it is based on LEFM. For example, for the Carrara marble at 250 °C, it is observed that methods based on LEFM, like SED criterion or TCD, do not provide satisfactory predictions.

In general, the TCD and the SED provide similar failure load predictions, especially when the critical strain energy density is calibrated to consider the small non-linearities of the tensile stress–strain curves. One of the main advantages of the SED criterion is that the strain energy density can be easily evaluated numerically through finite element analyses by using coarse meshes, and, although it is not the purpose of this work, it permits to take into account higher order terms and three-dimensional effects (e.g., Refs. 64, 65). Besides, once the  $H$  function is tabulated numerical analyses are no longer required and failure load predictions can be directly performed. By contrast, the main disadvantage compared to the TCD is that additional tests are required (i.e., uniaxial compression tests with strain gauge measurements), since the deformational parameters are needed. Based on the results, differences in the fracture load predictions obtained by the SED criterion and the TCD do not justify the additional workload involved by the SED approach. Indeed, the workload and cost of measuring the Young's modulus and the Poisson's ratio at temperatures above approximately 70 °C is substantial because special (and more expensive) strain gauges, adhesives and wires are required. Additionally, the complexity of performing the uniaxial compression tests at high temperatures compared to those at room temperature is also important.

## 6. Conclusions

This work studies the fracture behaviour of four different rocks with U-shaped notches subjected to mode I loading and to different temperature conditions by means of the SED criterion. To this end, the influence of temperature on the main mechanical

properties of the rocks has been studied, in particular the tensile strength ( $\sigma_t$ ), the fracture toughness ( $K_{IC}$ ), the compressive strength ( $\sigma_c$ ), the Young's modulus ( $E$ ), the Poisson's ratio ( $\nu$ ) and the thermal expansion. The results are based on an exhaustive and systematic laboratory campaign, which offers a new valuable database on the fracture properties of a sandstone, a limestone and two different marbles at different temperatures up to 250 °C, which is a common range in geothermal applications.

In the case of the Floresta sandstone (F) and the Moleano limestone (C), those rocks presenting a certain porosity, the tensile strength increases up to a certain critical temperature, after which it decreases. The increment in the tensile strength has been related to the closure of the pre-existing pores and microcracks due to the thermal expansion of the grains and water desorption. Likewise, the subsequent tensile strength reduction is caused by the appearance of new, thermally induced microcracks as a consequence of the differential thermal expansion of adjacent mineral particles. In the case of the Macael (M) and the Carrara marble (I), there is no internal space for the expansion of the grains. Thus, the tensile strength reduces from the onset of the heating process. On the other hand, the fracture toughness shows relatively similar trends to the tensile strength, since the main mechanisms also affect the mode I loading (opening) case. However, the critical temperature after which the fracture toughness decreases (in the sandstone and the limestone) has not been captured for the studied range of temperatures.

The compressive strength shows a generalised decrease with temperature in all the studied rocks except for the Moleano limestone (C), which displays a completely opposite behaviour up to 250 °C. Similarly, homologous trends are observed in the influence of temperature on the Young's moduli of the rocks. However, the  $E$  values of the marbles present a relatively marked drop while the reduction of the  $E$  of the sandstone is almost negligible. With regards to the Poisson's ratio, the four rocks show a decrement up to approximately 70 °C. Then, both marbles present a significant rise up to 250 °C (probably because of the observed non-linearities), while the Poisson's ratio values of the sandstone and the limestone remain roughly constant.

The proper characterisation of the main mechanical properties of the rocks, together with the application of the SED criterion, has led to relatively accurate fracture load predictions at the different temperature conditions and for different notch radii, avoiding the use of numerical modelling. The applied methodology assumes linear-elastic behaviour of the rocks throughout the range of considered temperatures. Both the Floresta sandstone (F) and the Moleano limestone (C) behave as quasi-brittle materials even at 250 °C. However, the analysed marbles reveal a significant influence of temperature on the stress-strain curves and present a certain degree of ductility as the temperature gets higher, even at room temperature in the particular case of the Carrara marble (I). As a consequence, the failure load predictions become less accurate when non-linearities gain a certain relevance.

### CRedit authorship contribution statement

**J. Justo:** Conceptualization, Methodology, Software, Formal analysis, Investigation, Writing - original draft, Visualization. **J. Castro:** Conceptualization, Methodology, Formal analysis, Investigation, Writing - review & editing, Supervision, Funding acquisition, Project administration.

### Declaration of competing interest

The authors declare that they have no known competing financial interests or personal relationships that could have appeared to influence the work reported in this paper.

### Acknowledgements

The authors of this work would like to express their gratitude to the Spanish Ministry of Economy and Competitiveness and to the European Regional Development Fund (ERDF) for financing the National Plan Project (Ref.: BIA2015-67479-R) under the name of "The Critical Distance in Rock Fracture", as well as to the Department of Universities and Research, Environment and Social Policy of the Government of Cantabria, for financing the Project "Characterization of the fracture process in rocks for geothermal applications". The authors would also like to thank J. de la Fuente and E. Gútez, technicians in the Geotechnical Research Group, and A. Lagüera, A. Jaurrieta and E. González Rauter, Civil Engineering students, for their help with the laboratory work.

### Appendix A

Appendix A gathers, respectively, the individual results of the tensile strength (Table 8), the fracture toughness (Table 9), the compressive strength (Table 10), the Young's modulus (Table 11) and the Poisson's ratio (Table 12), obtained from the laboratory campaign for each rock and temperature.

### Appendix B

In order to expand the  $H$  values for higher Poisson's ratios, second order polynomial trendlines have been considered, since they offer a good agreement. Fig. 15 represents as an example the individual values of  $H$  for each  $\nu$  (for the case of  $R_c/\rho = 0.05$ ) and the corresponding trendline. The extrapolated values of  $H$  are calculated by the obtained second order polynomial function in each case. The obtained relative error of those values calculated by the polynomial function compared to those in Table 1 is less than 0.02% in all the cases.

For the extrapolation of the  $H$  values for higher  $R_c/\rho$  ratios, some considerations must be taken into account. In the extreme case of analysing a crack with a radius equal to zero ( $\rho = 0$  mm),

**Table 8**

Individual test results of the tensile strength (in MPa) for each of the analysed rocks and temperatures. F: Floresta sandstone; C: Moleano limestone; M: Macael marble; I: Carrara marble.

	23 °C	70 °C	110 °C	150 °C	200 °C	250 °C
(F)	2,717	3,177	4,317	2,38	4,214	2,576
	3,279	2,896	4,767	3,241	2,381	3,379
	3,201	3,624	3,252	2,58	2,849	3,879
	2,306	3,075	3,752	3,789	4,078	3,472
	3,126	3,495	3,192	3,799	3,543	3,663
	2,42	-	3,636	3,228	2,752	4,298
(C)	6,822	7,172	10,607	9,45	8,805	8,271
	7,753	8,064	7,654	10,916	8,04	9,704
	7,08	8,611	9,495	9	10,011	8,667
	7,685	8,487	6,848	8,859	9,411	9,206
	6,998	8,222	10,31	9,013	8,602	8,802
	4,801	8,495	9,231	10,462	8,917	8,656
(M)	10,067	7,305	6,158	4,899	4,434	4,343
	9,935	7,822	6,256	5,567	4,084	4,679
	10,086	8,222	5,98	4,319	4,441	4,591
	9,847	8,23	6,081	4,731	4,662	5,413
	9,423	6,871	6,56	5,09	5,475	4,252
	10,439	6,689	6,454	4,895	5,124	3,743
(I)	9,133	7,201	5,69	6,129	3,583	4,098
	8,941	7,529	6,198	5,316	4,307	4,983
	9,761	7,358	4,859	4,839	4,453	4,673
	9,927	6,589	6,224	6,825	4,364	4,982
	7,932	8,229	5,925	5,962	3,599	5,829
	9,245	6,652	6,513	4,945	4,189	5,436

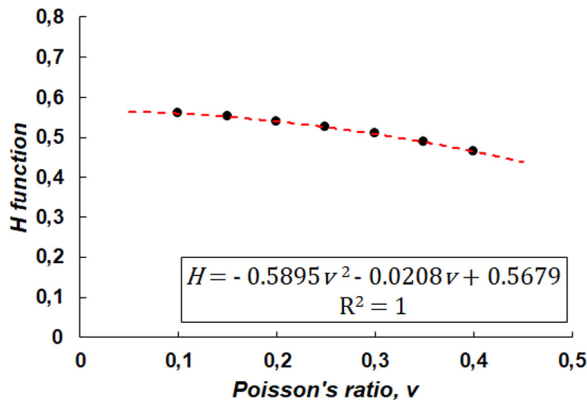


Fig. 15. Second order polynomial adjustment for  $R_c/\rho = 0.05$ .

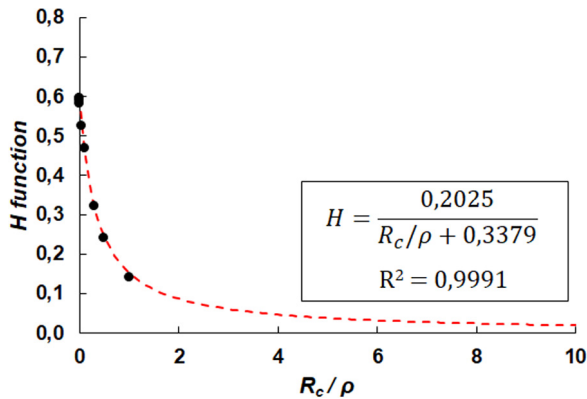


Fig. 16. First order rational adjustment for  $\nu = 0.25$ .

**Table 9**  
Individual test results of the fracture toughness (in  $\text{MPa m}^{1/2}$ ) for each of the analysed rocks and temperatures. F: Floresta sandstone; C: Moleano limestone; M: Macael marble; I: Carrara marble.

	23 °C	70 °C	150 °C	250 °C
(F)	0.421	0.389	0.362	0.309
	0.372	0.381	0.488	0.465
	0.277	0.500	0.524	0.562
	0.316	0.337	0.528	0.466
	0.434	0.469	0.349	0.455
	0.394	0.477	0.500	0.451
(C)	0.700	0.987	1.084	1.074
	0.640	0.937	0.939	0.989
	0.940	0.885	0.834	-
	0.650	-	0.892	0.922
	0.680	0.946	0.873	-
	0.780	1.030	1.067	1.310
(M)	1.190	1.046	0.462	0.593
	0.939	1.469	0.636	0.800
	1.187	1.309	0.574	0.831
	1.301	0.952	0.530	0.567
	1.169	0.873	0.656	0.714
	1.035	1.315	0.530	0.815
(I)	0.675	0.539	0.592	0.842
	0.873	0.770	0.680	0.510
	0.557	0.838	0.466	0.397
	0.678	0.806	0.608	0.433
	0.775	0.935	0.696	0.406
	0.904	0.633	0.654	0.424

**Table 10**

Individual test results of the uniaxial compressive strength (in MPa) for each of the analysed rocks and temperatures. F: Floresta sandstone; C: Moleano limestone; M: Macael marble; I: Carrara marble.

	23 °C	70 °C	150 °C	250 °C	
(F)	50,71	51,31	48,1	43,62	40,68
	50,53	54,02	37,31	-	35,64
	48,4	49,54	46,02	37,04	41,54
	51,06	47,05	48,07	40,13	36,03
	55,61	47,99	42,67	49,08	41,73
	-	48,63	40,54	33,2	54,67
(C)	60,51	82,49	-	107,54	141,13
	77,4	85,65	93,77	95,14	154,54
	-	79,48	88,91	148,99	110,83
	82,09	83,89	100,59	101,26	120,8
	82,88	81,85	86,27	106,63	112,45
	65,85	84,17	76,83	86,96	125,49
(M)	-	88,42	72,03	59,85	60,1
	90,22	69,46	64,14	70,55	57,32
	91,86	87,86	76,55	58,04	51,87
	69,84	94,83	67	63,94	65,86
	93,9	89,61	73,68	59,39	60,75
	85,47	91,47	77,34	54,92	58,09
(I)	91,33	98,31	85,26	76,22	71,41
	101,08	92,38	85,1	65,95	66,37
	97,07	102,9	77,39	73,15	63,18
	94,18	101,06	88,69	72,78	64,2
	97,86	93,54	93,83	73,387	64,54
	105,97	97,87	90,82	71,994	72,34

**Table 11**

Individual test results of the Young's modulus,  $E_{50}$  (in GPa) for each of the analysed rocks and temperatures. F: Floresta sandstone; C: Moleano limestone; M: Macael marble; I: Carrara marble.

	23 °C	70 °C	150 °C	250 °C	
(F)	20,7	19,3	17,5	18,9	16,5
	20,9	21,3	17,9	-	14,4
	18,8	20,2	20,3	14,0	18,0
	19,9	16,7	18,8	19,2	16,5
	22,8	16,5	19,5	16,6	17,4
	-	17,6	17,1	19,2	20,6
(C)	42,8	38,8	-	39,5	66,0
	40,3	34,8	45,4	43,2	61,7
	-	26,2	44,9	61,2	35,7
	40,0	43,3	47,4	35,8	33,1
	37,1	39,7	43,9	38,8	35,6
	37,9	41,5	41,4	37,9	63,2
(M)	-	68,1	65,1	28,4	20,0
	70,7	70,5	47,4	37,8	15,2
	88,0	78,7	54,9	25,2	20,5
	63,3	70,5	50,2	32,4	23,5
	70,1	73,7	56,8	26,5	20,9
	70,9	83,0	61,0	25,9	16,4
(I)	50,6	59,2	44,8	30,8	17,7
	57,8	57,6	53,1	23,4	18,1
	59,9	59,4	50,6	27,0	15,5
	51,9	59,3	50,2	28,2	15,9
	51,6	56,9	50,5	-	18,2
	62,3	59,0	51,1	-	19,2

both  $R_c/\rho$  and the maximum stress at the tip tend to infinite. In this situation  $H$  should be zero in order to accomplish Eq. (9). In the opposite case of an infinite notch radius ( $\rho = \infty$  mm), the specimen would develop a certain resistance and the maximum stress would have a finite value. Thus,  $H$  should also have a finite value according to Eq. (9). These conditions imply that the best-fit equation must have a horizontal asymptote for  $H = 0$  and must cut the vertical axis for  $R_c/\rho = 0$  in a certain finite value. Among all the possible equations meeting these conditions a rational equation of order 1 has the simplest form, since only

**Table 12**

Individual test results of the Poisson's ratio,  $\nu_{50}$  for each of the analysed rocks and temperatures. F: Floresta sandstone; C: Moleano limestone; M: Macael marble; I: Carrara marble.

	23 °C	70 °C	150 °C	250 °C
(F)	0,297	0,411	0,280	0,335
	0,405	0,347	0,319	–
	0,355	0,324	0,252	0,314
	0,349	0,340	0,336	0,312
	0,423	0,374	0,346	0,342
	–	0,325	0,227	0,303
(C)	0,412	0,245	–	0,260
	0,251	0,333	0,278	0,318
	–	0,256	0,255	0,298
	0,315	0,326	0,286	0,275
	0,275	0,360	0,289	0,253
	0,330	0,326	0,266	0,286
(M)	–	0,289	0,308	0,282
	0,347	0,270	0,261	0,333
	0,289	0,333	0,326	0,429
	0,479	0,451	0,294	0,262
	0,333	0,354	0,225	0,427
	0,347	0,345	0,248	0,393
(I)	0,388	0,350	0,297	0,340
	0,297	0,357	0,337	0,288
	0,299	0,353	0,308	0,282
	0,356	0,337	0,357	0,329
	0,333	0,400	0,237	–
	0,410	0,333	0,248	–

**Table 13**

Obtained best-fit parameters from Eq. (13) and the corresponding coefficient of determination ( $R^2$ ) for each rock and temperature. F: Floresta sandstone; C: Moleano limestone; M: Macael marble; I: Carrara marble.

	TEMP. (°C)	$\nu$	$a$	$b$	$R^2$
(F)	23	0.359	0.1727	0.3100	0.9989
	70	0.293	0.1914	0.3275	0.9990
	150	0.321	0.1838	0.3204	0.9990
	250	0.335	0.1797	0.3166	0.9989
(C)	23	0.312	0.1864	0.3229	0.999
	70	0.275	0.1963	0.3321	0.9991
	150	0.282	0.1945	0.3304	0.9990
	250	0.282	0.1944	0.3303	0.9990
(M)	23	0.349	0.1758	0.3129	0.9989
	70	0.277	0.1957	0.3316	0.9991
	150	0.354	0.1742	0.3113	0.9989
	250	0.421	0.1533	0.2911	0.9986
(I)	23	0.351	0.1751	0.3123	0.9989
	70	0.297	0.1904	0.3266	0.9990
	150	0.310	0.1869	0.3233	0.9990
	250	0.468	0.1375	0.2748	0.9983

two parameters are required<sup>13</sup>:

$$H = \frac{a}{R_c/\rho + b} \quad (13)$$

$a$  and  $b$  are obtained for each value of the Poisson's ratio from the best adjustment of the rational function shown in Eq. (13). The specific case of the rational best-fit curve for  $\nu = 0.25$  is represented in Fig. 16 as an example. A good agreement is observed between the tabulated  $H$  values (the dots) and the best-fit rational curve (the dotted line).

The best-fit parameters  $a$  and  $b$  have been obtained for the particular values of  $\nu$  corresponding to each of the analysed rocks and temperatures. These parameters have been collected in Table 13 together with the coefficient of determination ( $R$ -square) of each adjustment, and they allow the required  $H$  function to be calculated.

## References

- Li X, Wang E, Li Z, Liu Z, Song D, Qiu L. Rock burst monitoring by integrated microseismic and electromagnetic radiation methods. *Rock Mech Rock Eng.* 2016;49(11):4393–4406.
- Pearson CF, Fehler MC, Albright JN. Changes in compressional and shear wave velocities and dynamic moduli during operation of a hot dry rock geothermal system. *J Geophys Res - Sol Ea.* 1983;88:3468–3475.
- Sundberg J, Back PE, Christiansson R, Hökmark M, Ländell M, Wrafter J. Modelling of thermal rock mass properties at the potential sites of a Swedish nuclear waste repository. *Int J Rock Mech Min Sci.* 2009;46(6):1042–1054.
- Nasser MHB, Schubnel A, Young RP. Coupled evolutions of fracture toughness and elastic wave velocities at high crack density in thermally treated westerly granite. *Int J Rock Mech Min Sci.* 2007;44(4):601–616.
- Ramspott LD, Ballou LB, Carlson RC, et al. *Technical Concept for a Test of Geologic Storage of Spent Reactor Fuel in the Climax Granite, Nevada Test Site.* California Univ. Livermore, CA (United States), Lawrence Livermore Lab; 1979.
- Ranjith PG, Viete DR, Chen BJ, Perera MSA. Transformation plasticity and the effect of temperature on the mechanical behaviour of hawkesbury sandstone at atmospheric pressure. *Eng Geol.* 2012;151(151):120–127.
- McClure S, Horn RN. An investigation of stimulation mechanisms in enhanced geothermal systems. *Int J Rock Mech Min Sci.* 2014;72:242–260.
- Sirdesai NN, Singh TN, Ranjith PG, Singh R. Effect of varied durations of thermal treatment on the tensile strength of red sandstone. *Rock Mech Rock Eng.* 2017;50:205–213.
- Heuze FE. High-temperature mechanical, physical and thermal properties of granitic rocks – a review. *Int J Rock Mech Min.* 1983;20(1):3–10.
- Feng G, Kang Y, Chen F, Liu YW, Wang XC. The influence of temperatures on mixed-mode (I + II) and mode-II fracture toughness of sandstone. *Eng Fract Mech.* 2018;189:51–63.
- Araújo RGS, Sousa JLAO, Bloch M. Experimental investigation on the influence of temperature on the mechanical properties of reservoir rocks. *Int J Rock Mech Min Sci.* 1997;34. 298.e1–298.e16.
- Dongming Z, Yushun Y. The effect of high temperature on tensile strength and damage characteristics of limestone. *Geotech Geol Eng.* 2018;36:3527–3535.
- Justo J, Castro J, Cicero S. Notch effect and fracture load predictions of rock beams at different temperatures using the theory of critical distances. *Int J Rock Mech Min Sci.* 2020;125:104161.
- Duclos R, Paquet J. High-temperature behaviour of basalts – role of temperature and strain rate on compressive strength and K<sub>1c</sub> toughness of partially glassy basalts at atmospheric pressure. *Int J Rock Mech Min Sci Geomech Abstr.* 1991;28:71–76.
- Zhang LY, Mao XB, Lu AH. Experimental study of on the mechanical properties of rocks at high temperature. *Sci China Ser E.* 2009;52:641–646.
- Paterson MS, Wong TF. *Experimental Rock Deformation – The Brittle Field.* New York: Springer; 2005.
- Heap MJ, Baud P, Meredith PG. Influence of temperature on brittle creep in sandstones. *Geophys Res.* 2005;36:L19305.
- Al-Shayea N. Comparing reservoir and outcrop specimens for mixed mode I-II fracture toughness of a limestone rock formation at various conditions. *Rock Mech Rock Eng.* 2002;34(4):271–297.
- Meredith PG, Atkinson BK. Fracture toughness and subcritical crack growth during high-temperature tensile deformation of Westerly granite and Black gabbro. *Phys Earth Planet Inter.* 1985;39(1):33–51.
- Xu XC, Liu QS. A preliminary study on basic mechanical properties for granite at high temperature. *Chin J Geotech Eng.* 2000;22(3):332–335.
- Yang SQ, Ranjith PG, Jing HW, Tian WL, Ju Y. An experimental investigation on thermal damage and failure mechanical behavior of granite after exposure to different high temperature treatments. *Geothermics.* 2017;65:180–197.
- Justo J, Castro J, Cicero S, Sánchez-Carro MA, Husillos R. Notch effect on the fracture of several rocks: Application of the theory of the critical distances. *Theor Appl Fract Mech.* 2017;90:251–258.
- Gómez FJ, Guinea G, Elices M. Failure criteria for linear elastic materials with U-notches. *Int J Fract.* 2006;141:99–113.
- Gómez FJ, Elices M. A fracture criterion for sharp V-notched samples. *Int J Fract.* 2003;123:163–175.
- Berto F, Lazzarin P. Recent developments in brittle and quasi-brittle failure assessment of engineering materials by means of local approaches. *Mater Sci Eng.* 2014;75:1–48.
- Carpinteri A, Cornetti P, Pugno N, Sapora A, Taylor D. Generalized fracture toughness for specimens with re-entrant corners: experiments vs. theoretical predictions. *Struct Eng Mech.* 2009;32:609–620.
- Sapora A, Cornetti P, Carpinteri A, Firrao D. An improved finite fracture mechanics approach to blunt V-notch brittle fracture mechanics: experimental verification on ceramic, metallic, and plastic materials. *Theor Appl Fract Mech.* 2015;78:20–24.

28. Taylor D. Predicting the fracture strength of ceramic materials using the theory of critical distances. *Eng Fract Mech.* 2004;71:2407–2416.
29. Taylor D. *The Theory of Critical Distances: A New Perspective in Fracture Mechanics.* London: Elsevier; 2007.
30. Lazzarin P, Berto F. Some expressions for the strain energy in a finite volume surrounding the root of blunt V-notches. *Int J Fract.* 2005;135:161–185.
31. Berto F, Ayatollahi MR. Fracture assessment of Brazilian disc specimens weakened by blunt V-notches under mixed mode loading by means of local energy. *Mater Des.* 2011;32:2858–2869.
32. Torabi AR, Berto F, Campagnolo A, Akbaridoost J. Averaged strain energy density criterion to predict ductile failure of U-notched Al 6061-T6 plates under mixed mode loading. *Theor Appl Fract Mech.* 2017;91:86–93.
33. Lazzarin P, Zambardi R. A finite-volume-energy based approach to predict the static and fatigue behaviour of components with sharp V-shaped notches. *Int J Fract.* 2001;112:275–298.
34. Neuber H. *Kerbspannungslehre.* 2nd ed. Berlin: Springer-Verlag; 1958.
35. Berto F, Lazzarin P, Gómez FJ, Elices M. Fracture assessment of u-notches under mixed mode loading: two procedures based on the equivalent local mode I concept. *Int J Fract.* 2007;148:415–433.
36. Gómez FJ, Elices M, Berto F, Lazzarin P. Fracture of V-notched specimens under mixed mode (I + II) loading in brittle materials. *Int J Fract.* 2009;159:121–135.
37. Ayatollahi MR, Berto F, Campagnolo A, Gallo P, Tang K. Review of local strain energy density theory for the fracture assessment of V-notches under mixed mode loading. *Eng Solid Mech.* 2017;5(2):113–132.
38. Torabi AR, Campagnolo A, Berto F. Mode II brittle fracture assessment of key-hole notches by means of the local energy. *J Test Eval.* 2014;44(3):1261–1270.
39. Berto F, Ayatollahi MR, Borsato T, Ferro P. Local strain energy density to predict size-dependent brittle fracture of cracked specimens under mixed mode loading. *Theor Appl Fract Mech.* 2016;86:217–224.
40. Aliha MRM, Berto F, Mousavi A, Razavi SMJ. On the applicability of ASED criterion for predicting mixed mode I and II fracture toughness results of a rock material. *Theor Appl Fract Mech.* 2017;92:198–204.
41. Razavi SMJ, Aliha MRM, Berto F. Application of an average strain energy density criterion to obtain the mixed mode fracture load of granite rock tested with cracked asymmetric four-point bend specimens. *Theor Appl Fract Mech.* 2018;97:419–425.
42. Justo J, Castro J, Cicero S. Energy-based approach for fracture assessment of several rocks containing U-shaped notches through the application of the SED criterion. *Int J Rock Mech Min Sci.* 2018;110:306–315.
43. Berto F, Lazzarin P. A review of the volume-based strain energy density approach applied to V-notches and welded structures. *Theor Appl Fract Mech.* 2009;52:183–194.
44. Yosibash Z, Bussiba AR, Gilad I. Failure criteria for brittle elastic materials. *Int. J. Fract. Mech.* 2004;125(39):307–333.
45. Cicero S, Berto F, Ibáñez Gutiérrez FT, Procopio I, Madrazo V. SED Criterion estimations of fracture loads in structural steels operating at lower shelf temperatures and containing u-notches. *Theor Appl Fract Mech.* 2017;90:234–243.
46. ASTM D3967-16. *Standard Test Method for Splitting Tensile Strength of Intact Rock Core Specimens.* West Conshohocken, PA: ASTM International; 2016.
47. Coviello A, Lagioia R, Nova R. On the measurement of the tensile strength of soft rocks. *Rock Mech Rock Eng.* 2005;38(4):251–273.
48. UNE-EN 1926. *Natural Stone Test Methods – Determination of Uniaxial Compressive Strength.* AENOR; 2007 (in Spanish).
49. UNE-EN 14580. *Natural Stone Test Methods – Determination of Static Elastic Modulus.* AENOR; 2006 (in Spanish).
50. Ayatollahi MR, Bahrami B, Mirzaei AM, Yazid Yahya M. Effects of support friction on mode I stress intensity factor and fracture toughness in SENB testing. *Theor Appl Fract Mech.* 2019;103:102288.
51. Bahrami B, Ayatollahi MR, Mirzaei AM, Yazid Yahya M. Support type influence on rock fracture toughness measurement using semi-circular bending specimen. *Rock Mech Rock Eng.* 2020;53:2175–2183.
52. UNE-EN 13161. *Natural Stone Test Methods – Determination of Flexural Strength under Constant Moment.* AENOR; 2008 (in Spanish).
53. CEN/TS 14425-1. *Advanced Technical Ceramics – Test Methods for Determination of Fracture Toughness of Monolithic Ceramics – Part 1: Guide to Test Method Selection.* European: Committee for Standardization; 2003.
54. Zuo JP, Xie HP, Dai F, Ju Y. Three-point bending test investigation of the fracture behaviour of siltstone after thermal treatment. *Int J Rock Mech Min Sci.* 2014;70(9):133–143.
55. Dwivedi RD, Goel RK, Prasad VVR, Sinha A. Thermomechanical properties of Indian and other granites. *Int J Rock Mech Min Sci.* 2008;45:303–315.
56. Rao QH, Wang Z, Xie HF, Xie Q. Experimental study of properties of sandstone at high temperature. *J Cent South Univ Tech.* 2007;14:478–483.
57. Srawley J, Gross B. *Cracks and Fracture, Vol 601.* ASTM Spec. Tech. Publ; 1976:559–579.
58. Mahanta B, Singh TN, Ranjith PG. Influence of thermal treatment on mode I fracture toughness of certain Indian rocks. *Eng Geol.* 2016;210:103–114.
59. Chen YL, Shao W, Zhou YC. Experimental study on the influence of temperature on the mechanical properties of granite under uni-axial compression and fatigue loading. *Int J Rock Mech Min Sci.* 2012;56:62–66.
60. Tullis J, Yund RA. Experimental deformation of dry westerly granite. *J Geophys Res.* 1977;82:5705–5718.
61. Mao XB, Zhang LY, Li TZ, Liu HS. Properties of failure mode and thermal damage for limestone at high temperature. *Min Sci Tech.* 2009;19:290–294.
62. Bieniawski ZT, Bernede MJ. Suggested methods for determining the uniaxial compressive strength and deformability of rock materials: Part 2. suggested method for determining deformability of rock materials in uniaxial compression. *Int J Rock Mech Min Sci Geomech Abs.* 1979;16(2):138–140.
63. Creager M, Paris C. Elastic field equations for blunt cracks with reference to stress corrosion cracking. *Int J Fract.* 1967;3:247–252.
64. Pook LP, Berto F, Campagnolo A, Lazzarin P. Coupled fracture mode of a cracked disc under anti-plane loading. *Eng Fract Mech.* 2014;128:22–36.
65. Campagnolo A, Berto F, Lazzarin P. The effects of different boundary conditions on three-dimensional cracked discs under anti-plane loading. *Eur J Mech A-Solid.* 2015;50:76–86.